Kv7/KCNQ/M and HCN/h, but not $K_{Ca}2$/SK channels, contribute to the somatic medium after-hyperpolarization and excitability control in CA1 hippocampal pyramidal cells

Ning Gu, Koen Vervaeke, Hua Hu and Johan F. Storm

Institute of Basal Medicine, Department of Physiology, and Centre of Molecular Biology and Neuroscience, University of Oslo, PB 1103 Blindern, N-0317 Oslo, Norway

In hippocampal pyramidal cells, a single action potential (AP) or a burst of APs is followed by a medium afterhyperpolarization (mAHP, lasting ∼0.1 s). The currents underlying the mAHP are considered to regulate excitability and cause early spike frequency adaptation, thus dampening the response to sustained excitatory input relative to responses to abrupt excitation. The mAHP was originally suggested to be primarily caused by M-channels (at depolarized potentials) and h-channels (at more negative potentials), but not SK channels. In recent reports, however, the mAHP was suggested to be generated mainly by SK channels or only by h-channels. We have now re-examined the mechanisms underlying the mAHP and early spike frequency adaptation in CA1 pyramidal cells by using sharp electrode and whole-cell recording in rat hippocampal slices. The specific M-channel blocker XE991 (10 μM) suppressed the mAHP following 1–5 APs evoked by current injection at −60 mV. XE991 also enhanced the excitability of the cell, i.e. increased the number of APs evoked by a constant depolarizing current pulse, reduced their rate of adaptation, enhanced the afterdepolarization and promoted bursting. Conversely, the M-channel opener retigabine reduced excitability. The h-channel blocker ZD7288 (4-ethylphenylamino-1,2-dimethyl-6-methylaminopyrimidinium chloride; 10 μM) fully suppressed the mAHP at −80 mV, but had little effect at −60 mV, whereas XE991 did not measurably affect the mAHP at −80 mV. Likewise, ZD7288 had little or no effect on excitability or adaptation during current pulses injected from −60 mV, but changed the initial discharge during depolarizing pulses injected from −80 mV. In contrast to previous reports, we found that blockade of Ca^{2+}-activated K^+ channels of the SK/K_{Ca} type by apamin (100–400 nM) failed to affect the mAHP or adaptation. A computational model of a CA1 pyramidal cell predicted that M- and h-channels will generate mAHPs in a voltage-dependent manner, as indicated by the experiments. We conclude that M- and h-channels generate the somatic mAHP in hippocampal pyramidal cells, with little or no net contribution from SK channels.

(Resubmitted 18 March 2005; accepted after revision 5 May 2005; first published online 12 May 2005)
Corresponding author J. F. Storm: Department of Physiology at IMB and Centre for Molecular Biology and Neuroscience (CMBN), University of Oslo, PB 1103 Blindern, N-0317 Oslo, Norway. Email: jstorm@medisin.uio.no

In many excitable cells, action potentials are followed by afterpotentials that regulate the excitability of the cell for periods ranging from a few milliseconds up to several seconds. Afterpotentials that follow a single spike or a spike train can mediate different forms of feedback regulation of excitability.

Potassium (K^+) channels are particularly important for negative feedback regulation. Once activated by the action potentials (APs) – i.e. by the ensuing depolarization, Ca^{2+} influx, or both – K^+ channels mediate outward currents that outlast the APs and tend to hyperpolarize the cell, thus generating after-hyperpolarizations (AHPs). These AHP-generating K^+ currents are essential determinants of refractoriness, interspike interval durations and trajectories and, hence, spike timing, discharge patterns and discharge frequencies. In addition, inward currents evoked by spikes can generate afterdepolarizations (ADPs) that mediate positive feedback, thus facilitating extra spikes and bursts.

Neurones in the vertebrate CNS are equipped with a variety of AHP-generating K^+ currents and AHPs. A common pattern first described in hippocampal pyramidal cells (Storm, 1987*a*, 1990) is a sequence of three AHPs: (1) a fast one (fAHP, lasting 1–5 ms) that is a continuation of the

 DOI: 10.1113/jphysiol.2005.086835

spike repolarization; (2) a medium one (mAHP, typically lasting 50–200 ms), that mediates early spike frequency adaptation during a train of APs; and (3) a slow one (sAHP, lasting from about 0.5 s to several seconds) that mediates late spike frequency adaptation (Madison & Nicoll, 1984, Storm, 1990). In addition, a prominent ADP often occurs between the fAHP and mAHP (Kandel & Spencer, 1961; Storm, 1987*a*, 1990; Jensen *et al.* 1996; Yue & Yaari, 2004). In addition to mammalian hippocampal pyramidal cells (Lancaster & Nicoll, 1987; Storm, 1987*a*, 1990), a similar pattern is found in many other central neurones, e.g. pyramidal neurones in various layers of the mammalian neocortex (Schwindt *et al.* 1988) and amygdala (Pape & Driesang, 1998), in bulbar and spinal motoneurones (Takahashi, 1990; Viana *et al.* 1993) and in neurones of the striatum (Pineda *et al.* 1992).

Although this afterpotential pattern was first described almost two decades ago (Storm, 1987*a*), important issues remain partly unresolved or controversial, in particular regarding the mAHP mechanism. In contrast to the hippocampal sAHP, which has been studied in considerable detail (Madison & Nicoll, 1986; Madison *et al.* 1987; Lancaster & Nicoll, 1987; Pedarzani & Storm, 1993; Sah, 1996; Pedarzani *et al.* 1998), the mAHP has received relatively little attention, and seemingly conflicting interpretations persist. In particular, it is a widespread perception that the hippocampal mAHP is mediated largely by SK-type Ca^{2+}-activated K^+ channels (see reviews: Sah, 1996; Bond *et al.* 1999). For example, two recent studies support this notion (Stocker *et al.* 1999; Stackman *et al.* 2002), and apparently contradict previous studies that found no SK channel contribution to the mAHP (Storm, 1989; Williamson & Alger, 1990).

A second reason for re-examining the mAHP is that the molecular identity of the M-current (I_M) (Halliwell & Adams, 1982), which was originally proposed to be the main generator of the mAHP (Storm, 1989), has now been determined. The M-channels are made of subunits encoded by members of the Kv7 (KCNQ) family of K^+ channel genes (Wang *et al.* 1996). Hence, we use the term Kv7/KCNQ/M-channels. The M-channels of CA1 pyramidal cells are probably composed of Kv7.2 (KCNQ2), Kv7.3 (KCNQ3) and Kv7.5 (KCNQ5), subunits (Selyanko *et al.* 1999; Lerche *et al.* 2000; Shah *et al.* 2002). Furthermore, the importance of these channels for brain function and human disease has been elucidated (Jentsch *et al.* 2000; Jentsch, 2000). Mutations in the KCNQ2 and KCNQ3 genes cause hereditary forms of human epilepsy (benign familial neonatal convulsions; Biervert *et al.* 1998), and possibly also mental retardation (Borgatti *et al.* 2004). *In vitro* data also suggest that I_M is important for preventing bursting and epileptiform activity (Williamson & Alger, 1990; Yue & Yaari, 2004; Peters *et al.* 2005). Furthermore, I_M in CA1 pyramidal cells was recently shown to be an important mechanism for subthreshold electrical resonance in the theta frequency range – a likely mechanism of hippocampal theta oscillations (Hu *et al.* 2002*b*; Peters *et al.* 2005), which are strongly implicated in hippocampal memory formation and spatial navigation, and can enhance long-term synaptic plasticity (O'Keefe & Recce, 1993; Holscher *et al.* 1997; Jensen & Lisman, 2000; Dragoi *et al.* 2003). Kv7/KCNQ/M-channel genes are expressed in many parts of the brain that engage in slow oscillations (Cooper *et al.* 2001). Moreover, drugs developed as cognitive enhancers for treatment of Alzheimer disease and other memory disorders have turned out to be potent and rather selective blockers of Kv7/KCNQ/M-channels (Aiken *et al.* 1996). Recently, such channels have also been found in axons and presynaptic terminals, and implicated in axonal function and transmitter release (Martire *et al.* 2004; Devaux *et al.* 2004).

A third reason for re-examining the mAHP mechanism is that several new specific pharmacological tools for blocking or enhancing the currents putatively underlying the mAHP have become available. These include more selective and reliable M-channel blockers (Wang *et al.* 1998; Schnee & Brown, 1998) and openers (Main *et al.* 2000), SK-channel blockers (Johnson & Seutin, 1997) and h-channel blockers (Pape, 1994).

For these reasons, we have re-examined the mAHP mechanisms. We find that the mAHP of rat CA1 pyramidal cells is generated by Kv7/KCNQ/M-channels at depolarized membrane potentials and by HCN/h-channels at more negative potentials, with no detectable contribution from Ca^{2+}-activated K^+ channels. Some of these results have been presented in abstract form (Gu *et al.* 2003, 2004).

Methods

Slice electrophysiology

Transverse hippocampal slices (400 μm thick) were prepared from young adult male Wistar rats (3–8 weeks of age). The experimental procedures were approved by the responsible veterinarian of the Institute, in accordance with the statute regulating animal experimentation given by the Norwegian Ministry of Agriculture 1996. Briefly, the rats were deeply anaesthetized with Suprane before decapitation. Hippocampal slices (400 μm) were cut with a vibratome (Campden Instruments, UK) and maintained in an interface chamber filled with artificial cerebral spinal fluid (ACSF) containing (mM): 125 NaCl, 25 $NaHCO_3$, 1.25 KCl, 1.25 KH_2PO_4, 1.5 $MgCl_2$, 1.0 $CaCl_2$, 16 glucose and saturated with 95% O_2–5% CO_2. In experiments with Ca^{2+}-free medium, KH_2PO_4 was replaced by 1.25 mM KCl. During the recordings, the slices were kept submerged in a chamber perfused with ACSF of the composition described above, except that the $CaCl_2$ concentration was 2.0 mM. In a minority of the current-clamp experiments, 10 μM

DNQX (6,7-dinitroquinoxaline-2,3-dione) was added to the extracellular medium to block spontaneous excitatory synaptic transmission. The ACSF was saturated with 95% O_2/5% CO_2 and heated to 30°C. The temperature was kept constant within ±0.5°C during recording.

Intracellular recordings were obtained from CA1 pyramidal neurones with sharp electrodes filled with 2 mM potassium acetate (resistance 80–140 MΩ, pH 7.35). Whole-cell recordings from CA1 pyramidal neurones were established with the 'blind' method. The patch pipettes were filled with a solution containing (mM): 140 $KMeSO_4$ or potassium gluconate, 10 Hepes, 10 phosphocreatine sodium salt, 2 ATP sodium salt, 0.4 GTP sodium salt, and 2 $MgCl_2$, giving a pipette resistance of 4–7 MΩ. For current-clamp recordings, an Axoclamp 2A amplifier (Molecular Devices Corporation, Union City, USA) was used in bridge mode. The series resistance was 10–40 MΩ in whole-cell current-clamp recording. All potentials were corrected for the junction potential.

Only cells with a stable resting membrane potential more negative than −60 mV and stable AP amplitudes (>80 mV) were used for recording.

Data acquisition, storage and analysis

The data were acquired using pCLAMP 7.0 or 9.0 (Axon Instruments) at a sampling rate of 5–20 kHz, analysed and plotted with pCLAMP 9.0 and Origin 7.0 (OriginLab Corp.). Values are expressed as means ± S.E.M. Two-tailed Student's *t* test was used for statistical analysis ($\alpha = 0.05$). The *P* values are given in the figure legends.

The mAHP and sAHP amplitudes were measured by averaging the values within the time window (20 and 50 ms, respectively) around the peak of each AHP (20–100 ms and 0.1–3 s after a spike train, respectively). The cell input resistance was measured by injecting small (0.1–0.2 nA) hyperpolarizing current pulses (200 ms) and calculated by dividing the steady-state voltage response by the current pulse amplitude ($R_{input} = \Delta V / \Delta I$).

Chemicals and drugs

The M-channel blocker XE991 was obtained from DuPont pharmaceutical company. DNQX and ZD7288 (4-ethylphenylamino-1,2-dimethyl-6-methylaminopyrimidinium chloride) were purchased from Tocris Cookson (UK). Apamin was purchased from Latoxan (France). Retigabine was generously provided by Dr J. B. Jensen, Neurosearch, Copenhagen, Denmark. The remaining drugs were from Sigma-Aldrich, Norway AS (Oslo). Substances were bath-applied by adding them to the perfusion medium.

Computational methods

In the supplemental data (online address) we describe and motivate the CA1 pyramidal cell model in detail. Briefly, computer simulations were performed with the Surf-Hippo simulator, version 3.5a (Graham, 2004). The model is derived from the Borg-Graham CA1 pyramidal neurone model (Borg-Graham, 1999) that has been refined through collaborative studies by using our experimental data on discharge patterns, AHPs, subthreshold resonance and oscillations (Shao *et al.* 1999; Hu *et al.* 2002*b*, Gu *et al.* 2003). The cell was represented as a ball-and-stick type of model with five compartments: an isopotential soma (diameter 20 μm) and a dendritic cable (total length 800 μm and diameter 5 μm) consisting of four segments of equal length. This model combines intracellular Ca^{2+} dynamics with 11 active currents including persistent and transient Na^+ currents (I_{NaP}, I_{NaT}) (Borg-Graham, 1999), four voltage-gated K^+ currents (I_A, I_D, I_{DR}, I_M), a fast inactivating BK-type Ca^{2+}- and voltage-dependent K^+ current (I_{BK}) (Shao *et al.* 1999), two voltage-gated Ca^{2+} currents (I_{CaN} and I_{CaL}), a hyperpolarization-activated nonspecific cation current (I_h), and a Ca^{2+}-activated sAHP current (I_{sAHP}) (Borg-Graham, 1999).

Results

Current-clamp recordings were obtained from 117 CA1 pyramidal cells in strata pyramidale of rat hippocampal slices. In order to control for possible effects of different recording methods, both sharp electrode intracellular recordings ($n = 76$) and whole-cell patch-clamp recordings ($n = 41$) were used (see Methods). Except for a limited number of examples from other conditions, which are explicitly indicated in each case, the results presented are all from cells from young adult male rats (3–6 weeks), recorded with sharp electrodes or whole-cell patch-clamp (as indicated in the figure legends) in normal ACSF (with $[K^+]_o = 2.5$ mM and $[Ca^{2+}]_o = 2.0$ mM) at 30 ± 0.5°C.

The resting membrane potential (V_{rest}) and input resistance (R_{input}) were −65.0 ± 0.9 mV and 45.9 ± 2.3 MΩ for sharp electrode recordings, and −73.3 ± 1.1 mV and 51.4 ± 2.9 MΩ for whole-cell recordings, respectively.

Elimination of Ca^{2+} ions failed to affect the isolated mAHP

Figure 1 shows data from a typical intracellular recording from a rat CA1 pyramidal cell. The membrane potential was maintained at a slightly depolarized level, −60 mV, to enhance the amplitude of the mAHP. In order to test whether Ca^{2+}-activated K^+ channels contribute to the mAHP, we first eliminated the slow AHP (sAHP) by adding the adenylyl cyclase activator forskolin to the extracellular medium (Madison & Nicoll, 1986; Pedarzani & Storm, 1993) before exposing the slice to Ca^{2+}-free medium in which the Ca^{2+} was replaced by 2.0 mM Mn^{2+}) (see

Methods for details). As shown in Fig. 1*A* and *B*, the isolated mAHP amplitude was not significantly affected by the Ca^{2+}-free medium. Similar results were obtained in all five cells tested (summarized in Fig. 1*C*). In contrast, the decay time and waveform of the AP, monitored in parallel with the mAHP in the same cell, were clearly altered by the Ca^{2+}-free medium (Fig. 1*D* and *E*). The latter effect was expected as a consequence of suppression of currents through voltage-gated Ca^{2+} channels and Ca^{2+}-activated BK channels (Storm, 1987*a*). This confirmed that our application of Ca^{2+}-free medium with Mn^{2+} efficiently eliminated the activation of Ca^{2+}-activated channels in the same cell. The prior elimination of the sAHP by forskolin ensured that blockade of the sAHP by Ca^{2+}-free medium did not interfere with our measurements of the mAHP.

These results seem to indicate that Ca^{2+}-activated K^+ channels do not contribute significantly to the mAHP following a spike train, implying that SK channels, surprisingly (Stocker *et al.* 1999; Stackman *et al.* 2002), are not important for the mAHP in CA1 pyramidal cells.

The isolated mAHP is suppressed by M-channel blockade, but not by SK-channel blockade, at ∼−60 mV

Figure 2*A* shows the effect of forskolin and the M-channel blocker XE991 on the AHPs in a CA1 pyramidal neurone, activated from a background membrane potential of −60 mV (maintained by steady current injection). In normal ACSF (Fig. 2*A*1), a train of five APs, evoked by injection of a 50-ms-long current pulse, was followed by a mAHP lasting ∼80 ms, and a sAHP lasting more than 2 s. Bath application of forskolin (50 μM) fully suppressed the sAHP, thus leaving the mAHP in isolation (Fig. 2*A*2). Although forskolin often appeared to reduce the total AHP amplitude measured at the peak of the mAHP (Fig. 2*B*1, open triangle), this effect was most likely to be due to suppression of the overlapping early part of the sAHP. Thus, there appeared to be no obvious effect of forskolin on the mAHP *per se*.

The selective SK-channel blocker apamin (100 nM), when applied in the continued presence of forskolin, had

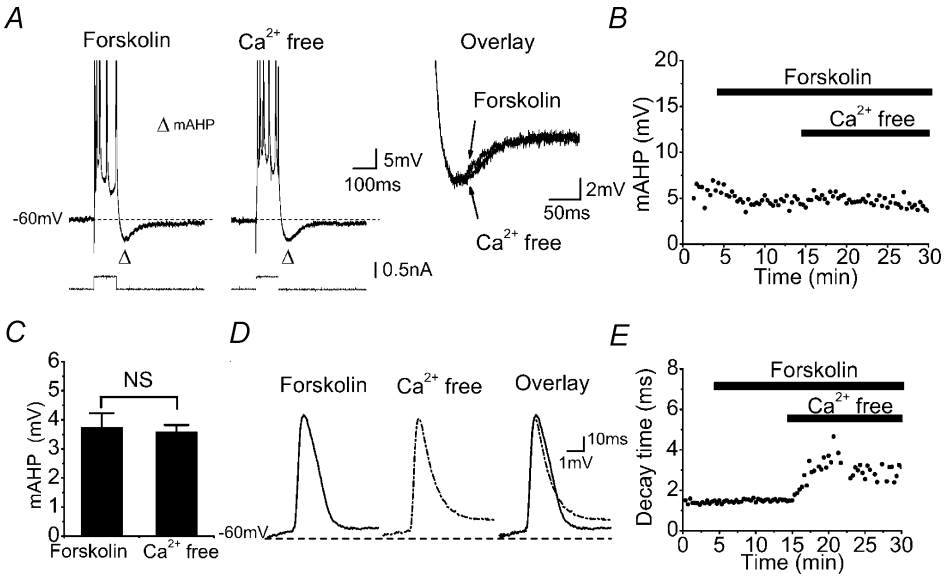

Figure 1. The mAHP in CA1 pyramidal neurones is not dependent on extracellular Ca^{2+}
A, intracellular sharp-electrode recording showing typical example of the medium afterhyperpolarization (mAHP) in a rat CA1 pyramidal cell recorded after inhibition of the slow AHP (sAHP) with bath-applied forskolin (50 μM). Subsequent application of Ca^{2+}-free extracellular medium with 2 mM Mn^{2+} caused no apparent change of the mAHP (overlay). The background membrane potential of the cell was kept at −60 mV by injecting steady depolarizing current. To evoke the mAHP and sAHP, a depolarizing current pulse was injected into the cell. The intensity of the current pulse was adjusted to evoke a constant number of action potentials (APs) per pulse (five). *B*, time course of the mAHP amplitude during the experiment shown in *A*. *C*, summary data showing the amplitude of mAHP before and after the application of Ca^{2+}-free medium in the presence of forskolin in five cells. *D*, typical example of an AP, before and after applying Ca^{2+}-free medium. Note that Ca^{2+}-free medium caused a dual effect on the spike repolarization, reflected as a narrowing of the upper ∼two-thirds and broadening of the lower ∼one-third of the spike. *E*, time course of AP 90–10% decay time, showing the effect of Ca^{2+}-free medium on spike repolarization during the experiment shown in *D*. *A*, *B*, *D* and *E* are records obtained from the same cell.

little or no effect on the mAHP (Fig. 2*A*3 and *B*2). In contrast, when the selective KCNQ/M-channel blocker XE991 (10 μM) was applied (in the continued presence of forskolin and apamin), the mAHP was fully suppressed and was replaced by an afterdepolarization (ADP) that lasted about 50 ms (Fig. 2*B*3). Figure 2*C* shows the time courses of the drug effects.

Essentially identical results to those presented in Fig. 2*A*–*C* were obtained in all CA1 pyramidal cells tested with this stimulation protocol in the presence of forskolin, followed by apamin ($n = 4$) and XE991 ($n = 4$). Figure 2*D* shows the summary data from all cells tested.

These results indicate that the mAHP is largely due to activation of I_M, with little or no contribution from SK channels (Storm, 1989). This hypothesis is consistent with the apparent lack of effect of forskolin on the mAHP (Fig. 2*A*1 and 2), since I_M is reported to be largely resistant to protein kinase A activation in CA1 pyramidal cells (Madison & Nicoll, 1986; Madison *et al.* 1987).

Robust SK currents in CA1 pyramidal cells

In view of the lack of effect of apamin described above, one might suspect that the SK channels for some reason

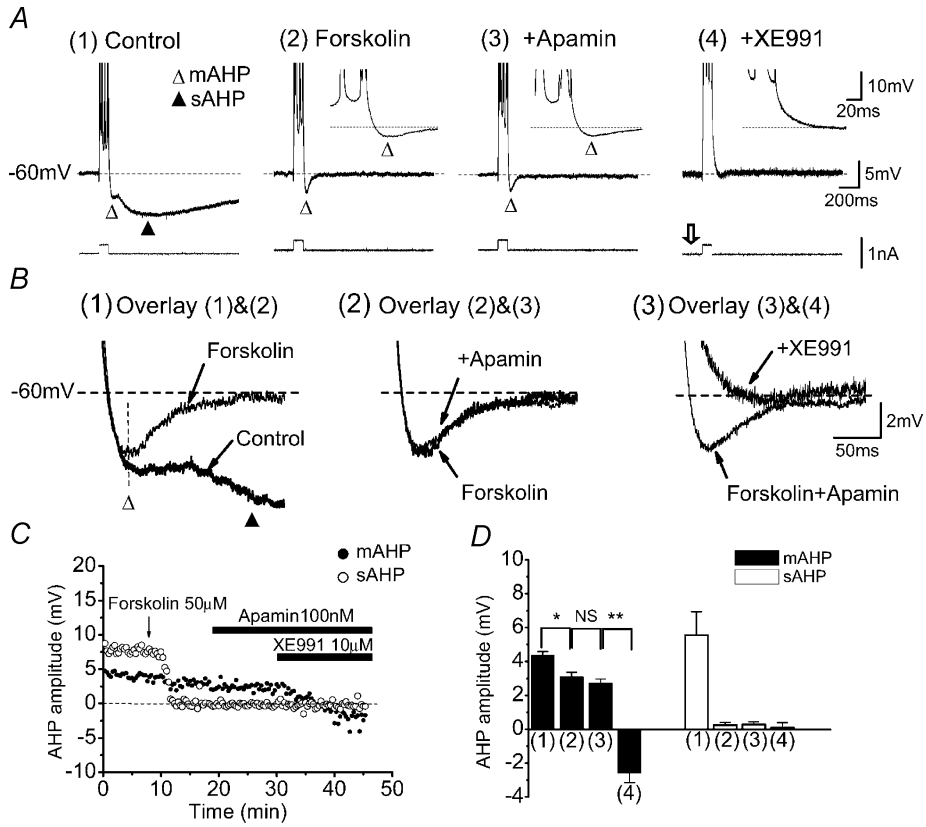

Figure 2. Effect of forskolin, apamin and XE991 on the mAHP and the sAHP
A, intracellular sharp electrode recording showing typical examples of the medium (mAHP, △) and slow (sAHP, ▲) afterhyperpolarizations in a CA1 pyramidal cell before (1) and after (2) bath-application of 50 μM forskolin, followed by 100 nM apamin (3), and then 10 μM XE991 (4). Inserts in *A*2 and 3 show the mAHP on an expanded scale. The background membrane potential of the cell was kept at −60 mV by injecting steady depolarizing current. XE991 caused the cell to depolarize, but this was compensated by decreasing the positive steady current (open arrow), thus keeping the membrane potential at −60 mV. To evoke the mAHP and sAHP, a depolarizing current pulse was injected into the cell. The intensity of the current pulse was adjusted to always evoke five APs per pulse. *B*, mAHP and sAHP traces from *A* are shown superimposed on an expanded scale: before and after forskolin (1), before and after apamin (2), before and after XE991 (3). Note that forskolin completely suppressed the sAHP, thereby also affecting the peak amplitude measurement of the mAHP (1, vertical dashed line). The latter effect is probably due to overlap of the mAHP and sAHP. In the presence of forskolin, the mAHP was unaffected by apamin (2), but was completely blocked and converted to an after-depolarization potential (ADP) by subsequent application of XE991 (3) (see also insert in *A*4). *C*, time course showing the effects of forskolin, apamin and XE991 on the amplitude of the mAHP (●) and sAHP (○) from the same cell as in *A* and *B*. *D*, summary graph showing the effect of forskolin, apamin and XE991 on the amplitude of the mAHP (filled columns) and sAHP (open columns) in all cells tested with these drugs ($n = 4$, $^*P < 0.05$, $^{**}P < 0.01$, NS $P > 0.05$).

might be downregulated (including 'run down') and thus unavailable for activation under our experimental conditions, or that our apamin or application procedure was ineffective. In order to test for these possibilities, we used an experimental protocol that is known to strongly activate SK channels (Sailer *et al.* 2002; Fig. 3*A*).

Figure 3*A* shows voltage-clamp recordings from a CA1 pyramidal cell, in which Na^+ channels and some K^+ channels have been blocked by tetrodotoxin (TTX, 1 μM) and tetraethylammonium (TEA, 5 mM), respectively. Under these conditions, a brief depolarizing voltage step evoked an unclamped Ca^{2+} spike (Pedarzani & Storm, 1993) followed by outward tail currents (Fig. 3*A*, control). Bath application of 100 nM apamin strongly reduced the early part of the outward tail current, thus identifying it as an SK current (Pennefather *et al.* 1985; Stocker *et al.* 1999; Sailer *et al.* 2002). In contrast, the late slow part of the tail current, I_{sAHP}, was resistant to apamin, in agreement with previous reports (Lancaster & Nicoll, 1987; Storm, 1989; Stocker *et al.* 1999).

Apamin had similar effects, with a convincing time course (Fig. 3*B*), in all cells tested in this manner ($n = 7$). Specifically, clear effects of apamin on the early tail current were seen also when the whole-cell recording prior to apamin application lasted longer (10 min; $n = 5$) than in the whole-cell current clamp experiments (without TTX or TEA) where apamin failed to affect the mAHP (6–8 min, $n = 9$, data not shown). These results indicate that the SK channels of CA1 pyramidal cells are available for activation, i.e. they are not lost or downregulated, under our recording conditions, and that our apamin applications effectively block these channels. Nevertheless,

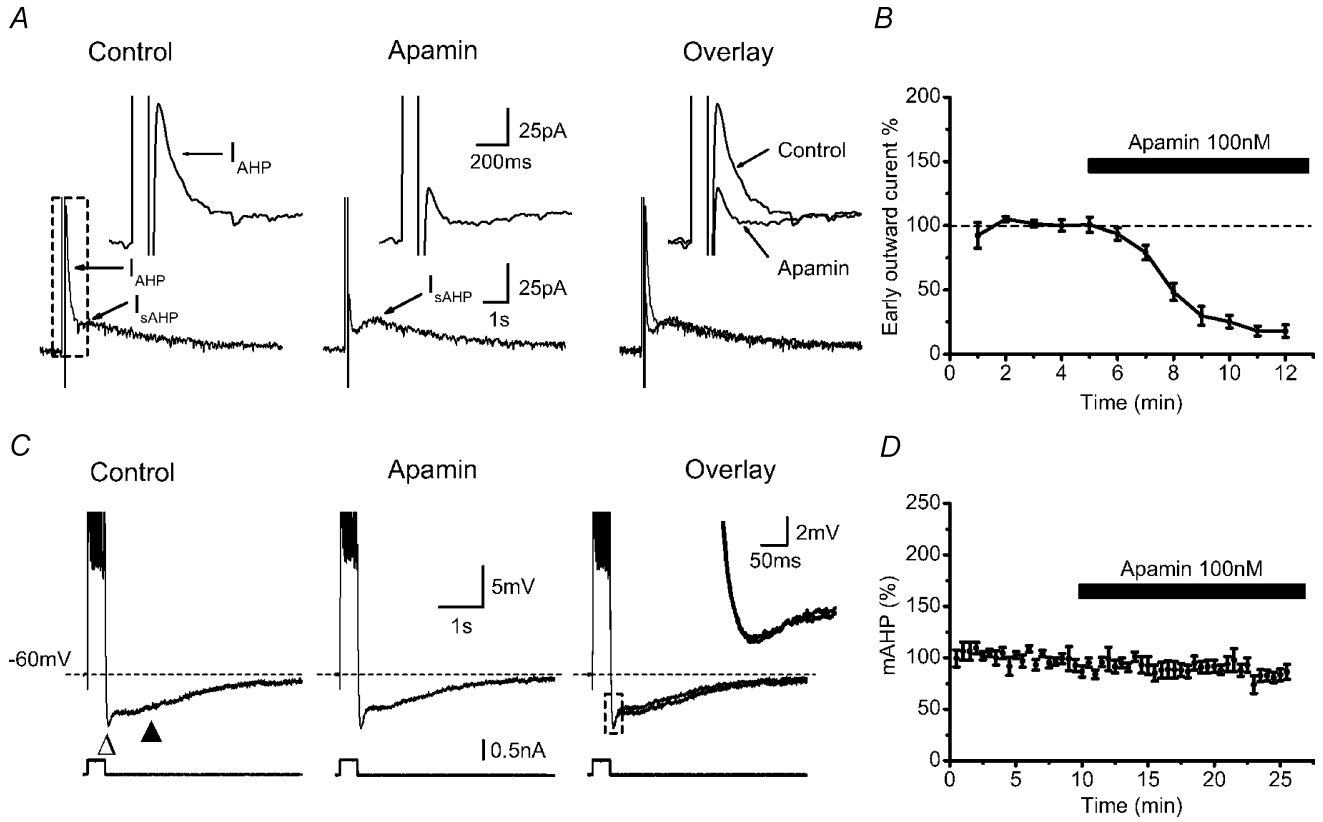

Figure 3. Apamin-sensitive AHP (SK) current can be evoked in the presence of TTX and TEA, but does not contribute to the mAHP in normal extracellular medium

A, typical example of afterhyperpolarization (AHP) current recorded with whole-cell voltage-clamp in CA1 pyramidal neurones. The cell was voltage clamped at −50 to −55 mV with 1 μM TTX and 5 mM TEA in the bath. A 100 ms voltage step of sufficient amplitude (usually to 0 mV) to trigger a Ca^{2+} spike was applied to the cell to evoke AHP currents. Note that the outward tail current following the voltage step contains two components with different kinetics: a fast component (I_{AHP}) of medium duration (~200 ms) and a slow component (I_{sAHP}) lasting several seconds. Apamin (100 nM) selectively inhibited I_{AHP}, sparing I_{sAHP}. The insets show I_{AHP} before and after apamin on expanded scales. *B*, summary data showing time course of the normalized I_{AHP} amplitude before and after apamin ($n = 7$). *C*, current-clamp recording obtained with a sharp intracellular electrode, showing that without the presence of TTX and TEA, the mAHP (△) following a 400 ms train of 10 APs can not be blocked by 100 nM apamin. The recording temperature was 23°C. *D*, averaged time course showing the application of the selective SK-channel blocker apamin (100 nM) had no apparent effect on mAHP amplitude. ($n = 6$, $P > 0.05$)

apamin consistently failed to affect the mAHPs, even following long-duration high-frequency spike trains as shown in Fig. 3*C* and *D* ($n = 6$, $P > 0.05$). Taken together, these results seem to indicate that SK channels, although available for activation, are not normally activated by spike trains in CA1 pyramidal cells.

M-channel blockade suppresses the mAHP, but not the sAHP

The experiments presented in Figs 1 and 2 have the advantage that they permit analysis of the mAHP in isolation, after suppression of the sAHP. However, they leave open the possibility that forskolin might alter the mAHP mechanism, e.g. by suppressing an otherwise important component of the mAHP while perhaps enhancing another. Although previous experiments indicate that SK channel activity is not affected (Varnum *et al.* 1993) or possibly even somewhat enhanced (Stocker *et al.* 1999) by protein kinase A activation, it is important to examine the mAHP also in the absence of artificial kinase activation.

Figure 4*A* and *C* shows the effect of XE991 on the mAHP and sAHP following a train of five APs in normal ACSF. XE991 (10 μM) fully suppressed the mAHP. In contrast, the sAHP was enhanced, most likely because the cell's R_{input} was increased, thus increasing the voltage deflection produced by the sAHP current. Similar results were obtained in all cells tested (Fig. 4*E*, $^{**}P < 0.01$, $n = 5$). Other experiments showed that muscarine (10 μM), which is known to suppress both I_M (Halliwell & Adams, 1982) and I_{sAHP} (Madison *et al.* 1987) through cholinergic receptor activation, abolished both the mAHP and sAHP. As the AHPs were blocked, an ADP appeared (Yue & Yaari, 2004). Similar results were obtained in all cells tested with muscarine ($n = 5$; data not shown), in close agreement with previous findings (Storm, 1989), thus further supporting the hypothesis that the mAHP, at membrane potentials close to −60 mV, is largely due to I_M.

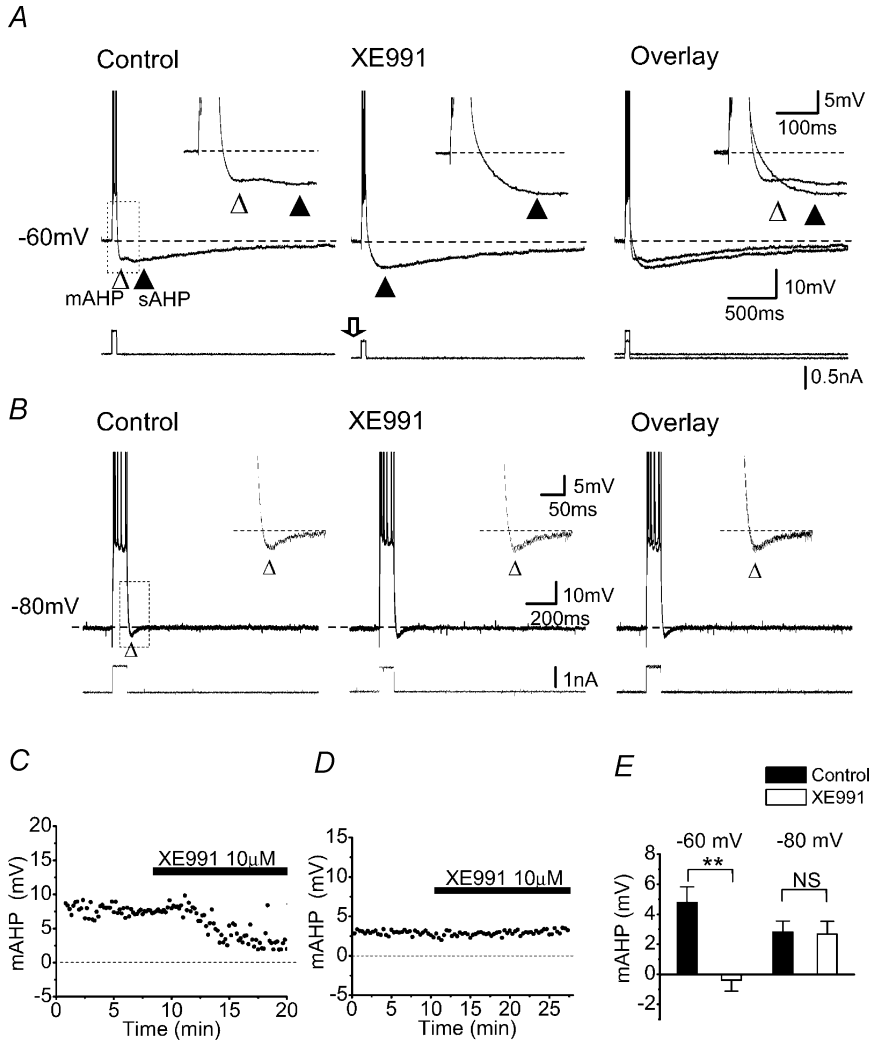

Figure 4. Blockade of I_M suppressed the mAHP at depolarized membrane potentials
A, whole-cell recording showing that blockade of M-current (I_M) by 10 μM XE991 selectively suppressed the mAHP (△) at a depolarized background membrane potential, −60 mV. Similar effects were seen in all five cells tested in this way. Note that the sAHP (▲) was enhanced by blocking I_M with XE991. The insets show the mAHP (from the dashed box) on an expanded scale. *B*, sharp electrode intracellular recording showing that blockade of I_M with XE991 had no apparent effect on the mAHP following a train of spikes evoked at a hyperpolarized background membrane potential −80 mV. The insets show the mAHP (dashed box) on expanded scales. The dashed lines in *A* and *B* indicate the membrane potential at which the neurones were maintained by constant current injection (−60 mV in *A*, and −80 mV in *B*). *C* and *D*, time courses from the experiments *A* and *B*, showing the XE911 effect on the mAHP amplitude while holding the membrane potential at −60 and −80 mV, respectively. *E*, summary data showing the voltage-dependent effect of XE991 on mAHP (at −60 mV, $n = 5$, $^{**}P < 0.01$; at −80 mV, $n = 5$, NS $P > 0.05$).

M-channel blockade failed to suppress the mAHP at ∼−80 mV

So far, the mAHP mechanisms were tested in cells whose background membrane potential was kept close to −60 mV by steady current injection (Figs 2, 4*A* and *C*). This was done to mimic an activated depolarized state, which is likely to occur often in pyramidal cells *in vivo* (Steriade *et al.* 1993; Buzsaki, 2002), and in which AHPs are likely to have their greatest impact. This condition also facilitates analysis of K^+ current contributions to the AHPs, since they are enhanced by the increased driving force for K^+. However, since the putative mAHP mechanisms are voltage dependent (Storm, 1989; Maccaferri *et al.* 1993; Hu *et al.* 2002*b*), we also studied the mAHP at different potentials. Figure 4*B* shows the effect of XE991 on the mAHP following a five-spike train at a background membrane potential (V_m) of −80 mV, maintained by steady current injection. At this potential, there was little or no apparent sAHP, presumably because V_m was close to the reversal potential for K^+ (E_K, calculated to be −105 mV under our whole-cell recording conditions). We found that XE991 had no effect on the mAHP at this potential (Fig. 4*B* and *D*), in striking contrast to its effect at ∼−60 mV (Fig. 4*A* and *C*), indicating that the mAHP at ∼−80 mV is not due to I_M. Similar results were obtained in all cells tested (Fig. 4*E*, $P > 0.05$ (NS), $n = 5$).

HCN/h-channel blockade suppressed the mAHP at ∼−80 mV, but not at ∼−60 mV

The observation that M-channel blockade failed to suppress the mAHP at highly negative potentials (Fig. 4*B* and *D*) is consistent with the hypothesis (Storm, 1989) that it is I_h, rather than I_M that generates the mAHP at these potentials. However, this hypothesis was largely based on the use of Cs^+ – a blocker that is not selective for I_h, but which also blocks inward-rectifier K^+ channels (Lesage *et al.* 1995; Mermelstein *et al.* 1998).

We therefore re-examined this issue by using the more selective h-channel blocker ZD7288. As shown in Fig. 5, ZD7288 (10 μM) had no consistent effect on the mAHP at −60 mV (Fig. 5*A* and *B*), but fully blocked the mAHP evoked at ∼−80 mV (Fig. 5*C* and *D*). It also abolished the I_h-induced depolarizing 'sag' in response to hyperpolarizing current pulses (Fig. 5*E* and *F*). Similar results were obtained in all cells tested with ZD7288 at −60 ($n = 5$) and −80 mV ($n = 5$), as illustrated by the summary graphs (Fig. 5*G* and *H*). These results strongly support the idea that the mAHP at highly negative membrane potentials is caused by I_h deactivation (Storm, 1989; Williamson & Alger, 1990; Maccaferri *et al.* 1993).

The mAHP following a single AP

It may appear dubious that such a slow current as I_M, which has activation time constants of up to several hundred milliseconds, can be activated appreciably by a single spike that last only about 1 ms (Goh & Pennefather, 1987; Storm, 1987*a*, 1989; Yue & Yaari, 2004). Nevertheless, each AP during slow repetitive firing in CA1 pyramidal cells is usually followed by a mAHP, and a similar mAHP is also evident after a single-pulse-evoked spike (Lanthorn *et al.* 1984; Storm, 1989). Such single-spike mAHPs are likely to play an important role in determining the relative refractory period, ISIs and, hence, the discharge frequency (Lanthorn *et al.* 1984; Madison & Nicoll, 1984; Storm, 1989, 1990).

To test whether the single-spike mAHP is caused by I_M, XE991 was applied to CA1 pyramidal cells that fired repetitively at a moderate rate (1–3 Hz) in response to injection of long-lasting (1–2 s) depolarizing current pulses. Figure 6*A* and *B* shows that 10 μM XE991 suppressed the mAHP following each single AP in the train: the mAHP following the first AP, evoked soon after the onset of the current pulse (Fig. 6*A*), as well as the later mAHP during steady-state repetitive firing (data not shown).

When a single AP was evoked by a brief current pulse, it was often followed by a prominent ADP, in addition to the mAHP, which appeared small in amplitude relative to the more negative membrane potential following it (Fig. 6*C* and *D*) (Kandel & Spencer, 1961; Storm, 1987*a*; Jensen *et al.* 1996). XE991 strongly enhanced the ADP, often causing it to elicit a regenerative burst of APs that outlasted the injected current pulse (Yue & Yaari, 2004). Similar effects were observed in all cells tested in these ways (Fig. 6*A* and *B*, *C* and *D*, $n = 5$ and 5, respectively), as illustrated by the summary graphs (Fig. 6*E* and *F*, $P < 0.01$ in each group).

Excitability control by I_M and I_h

In order to test how I_M affects excitability, we bath-applied 10 μM XE991 while injecting long current pulses (Fig. 7). XE991 caused a depolarization of V_{rest} and increased R_{input}, as indicated by increased voltage deflections to depolarizing and hyperpolarizing pulses of subthreshold intensities (Fig. 7*A*). These changes in V_{rest} and R_{input} will both tend to increase excitability, and such an increase was clearly observed in response to pulses of suprathreshold intensities. Thus, a current pulse that under normal conditions evoked only three spikes at low frequency, triggered a high-frequency burst of six spikes, followed by an enhanced sAHP (Fig. 7*B*, right, filled triangle) after application of XE991. To test how much of the excitability increase was due to the XE991-induced depolarization, we used direct current (DC) to readjust the background membrane potential back to the control

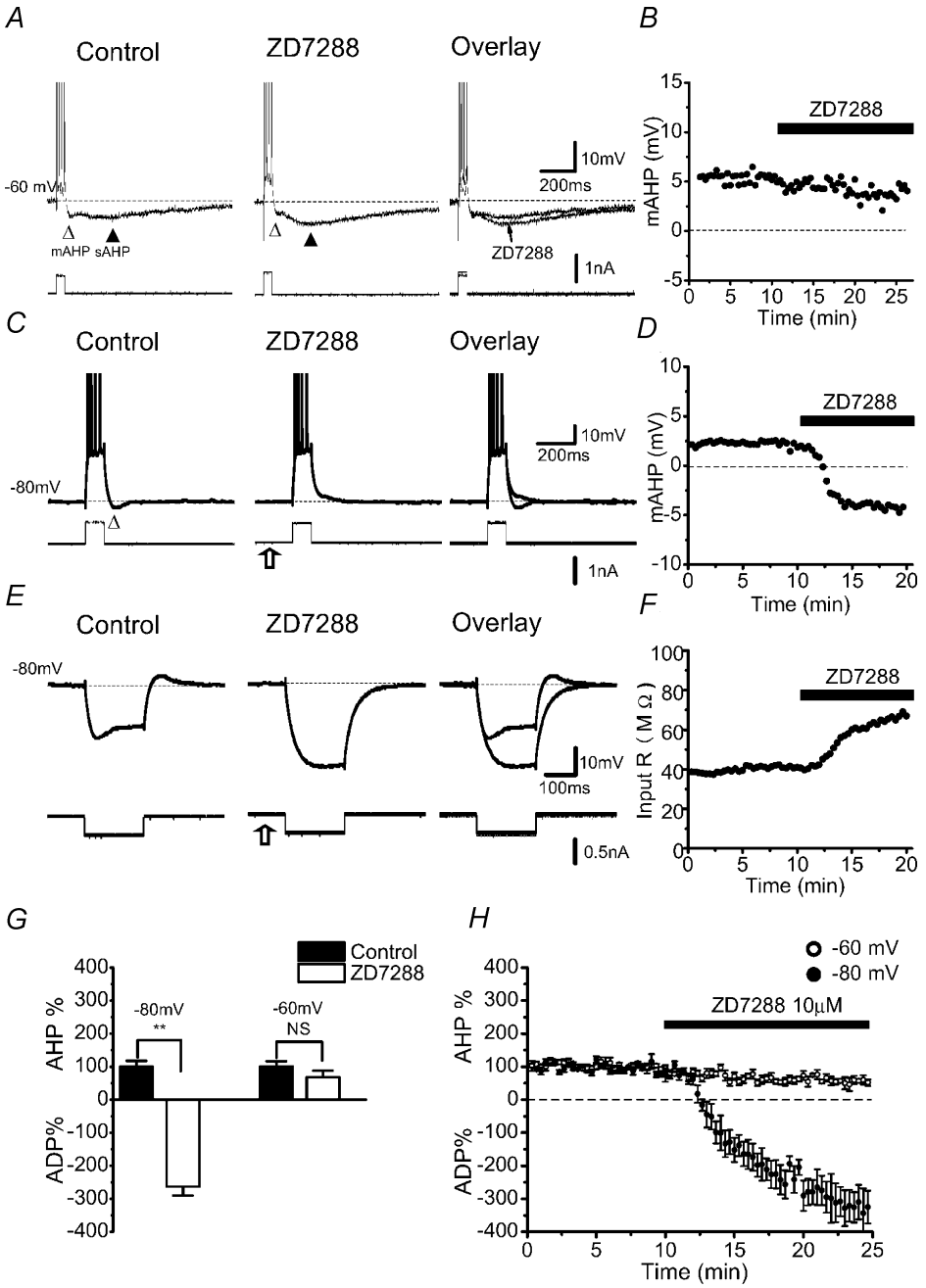

Figure 5. Blockade of h-current (I_h) suppressed the mAHP at hyperpolarized membrane potentials
A–D, the h-channel blocker ZD7288 (10 μM) suppressed the mAHP (△) at −80 mV (*C*) but not at −60 mV (*A*). *B* and *D*, time courses of the ZD7288 effect on the mAHP amplitude from the experiments shown in *A* and *C*, respectively. The example illustrated in *A* and *B* was from a sharp electrode intracellular recording; the one shown in *C* and *D* was obtained with whole-cell patch-clamp recording. Note that ZD7288 enhanced the sAHP (▲) (*A*), and caused the cell to hyperpolarize, which was compensated by increasing the positive steady current to keep the membrane potential at −80 mV (open arrow). *E*, ZD7288 (10 μM) inhibited the I_h-dependent 'sag' evoked by a hyperpolarizing current pulse and increased the input resistance at −80 mV. *F*, time course of the ZD7288 effect on the cell input resistance, measured at the end of each current pulse. *C* and *D*, and *E* and *F*, are from the same cell. *G*, summary data ($n = 10$) showing the voltage-dependent effect of ZD7288 on ADP and mAHP (NS $P > 0.05$, $^{**}P < 0.01$). *H*, normalized time course showing the average effect of ZD7288 on the mAHP and ADP at −60 mV (○) and at −80 mV (●).

level after applying XE991 (Fig. 7*C*). Also in this case, a current pulse that previously caused only a few APs at low frequency, evoked a high-frequency burst in the presence of XE991. Similar effects of XE991 as illustrated in Fig. 7*A–C* were observed in all 16 cells tested in these ways ($n = 5$, 5 and 6, respectively).

In contrast to XE991, apamin (100 nM) had no detectable effect on the number, frequency or pattern of APs, whereas XE991 applied after apamin again strongly increased the spike number and frequency (Fig. 7*D* and *E*) in all six cells tested (summary data, Fig. 7*F–H*). These data indicate that M-channels are very important for excitability control in CA1 pyramidal cells, whereas SK channels do not appear to contribute to excitability control or spike frequency adaptation in CA1 pyramidal cells under these experimental conditions.

We next tested whether I_h affects excitability. As illustrated in Fig. 8*A*, application of ZD7288 (10 μM) caused a hyperpolarization of the cell, and increased its R_{input}, presumably because a standing I_h and h-conductance were blocked. In the presence of ZD7288, the normal I_h-dependent over-/undershoot and sag

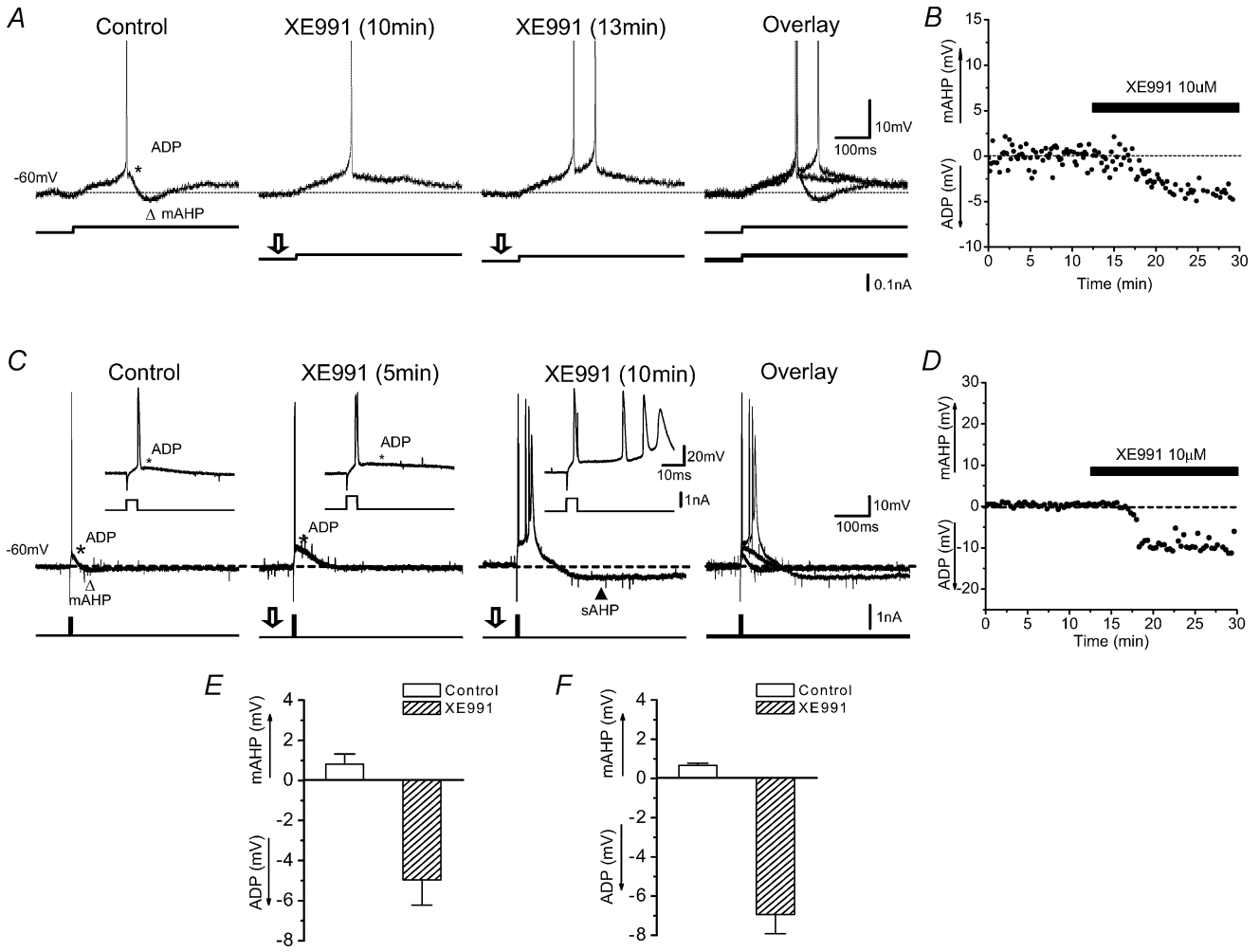

Figure 6. Effects of XE991 on the afterpotentials following a single AP
Sharp-intracellular-electrode recordings showing the ADP (∗) and mAHP (△) following a single AP. Each AP was evoked by injecting a long lasting (2 s, *A*) or brief (2 ms, *C*) depolarizing current pulse into the neurone, starting from a membrane potential of −60 mV (maintained by steady depolarizing current injection). *A*, application of 10 μM XE991 first inhibited the mAHP and enhanced the ADP (10 min after onset of XE991 application), and subsequently caused discharge of a second AP (spike doublet; 13 min). *C*, XE991 application caused blockade of the mAHP and enhancement of the ADP (after 5 min), leading to an all-or-none burst discharge (after 10 min). Note that XE991 also caused the membrane potential to depolarize. Therefore, less positive holding current was needed to maintain the same potential compared to the control situation (lower traces in *A*; $n = 10$, $P < 0.01$). The insets in *C* show the mAHP and the ADP on expanded scales. *B* and *D*, time courses of the XE991 effect on the mAHP amplitude from the experiments shown in *A* and *C*, respectively. *E* and *F*, summary graphs of the XE991 effects from two different groups of experiments shown in *A* and *C* (each group: $n = 5$, $P < 0.01$).

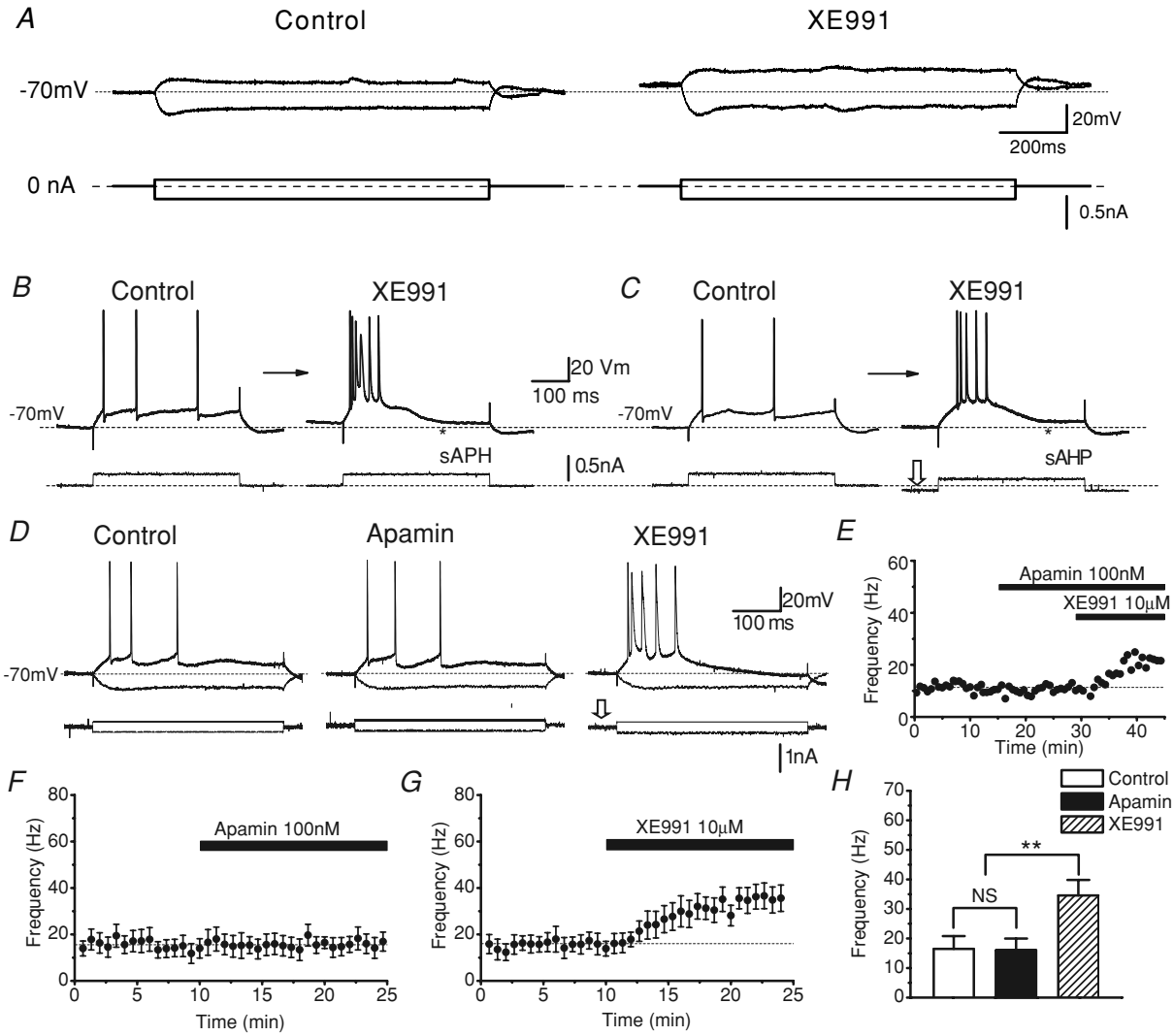

Figure 7. XE991, but not apamin, increased neuronal excitability and bursting
A, the M-channel blocker XE991 caused a depolarization of the resting membrane potential (V_{rest}), accompanied by an increase in the input resistance. Typical example from a whole-cell recording. The cell was at V_{rest} (−70 mV); current pulses (1 s duration) of opposite polarity were injected. *B* and *C*, sharp electrode intracellular recording showing that XE991 increased excitability and promoted burst firing. The background membrane potential was maintained at −70 mV by injecting steady current, and a depolarizing current pulse (0.3 nA, 400 ms duration) was injected every 20 s. Application of XE991 depolarized the cell, and transformed its response to a high-frequency burst followed by a sAHP (▲ in *B*). A similar burst response was also observed when the background depolarization caused by XE991 was reversed by adjusting the steady current injection (*C*). Similar results were obtained in all cells tested in these ways (*A*, $n = 5$; *B*, $n = 6$). *D*, XE991, but not apamin, increased the excitability of CA1 pyramidal cells; typical example from a sharp electrode intracellular recording. Responses to injection of 400-ms-long depolarization and hyperpolarizing current pulses of ±0.2 nA are shown superimposed. *E*, time course of changes in average AP frequency from the cell illustrated in *D*, before and after application of apamin followed by XE991. The AP frequency was calculated by averaging the instantaneous frequencies (i.e. 1/interspike interval) for all APs during each current pulse. *F* and *G*, summary time courses for all cells tested with apamin (*F*, $n = 5$) and XE991 (*G*, $n = 5$), showing the effects of these blockers on the average AP frequency. *H*, summary data, average AP frequencies resulting from application of apamin ($n = 5$) and XE991 ($n = 5$) *versus* normal medium prior to drug application (control) for all cells tested (**$P < 0.01$; NS $P > 0.05$).

pattern (Fig. 8*A*, left) was replaced by a more linear response to hyperpolarizing current pulses, and a slow ramp in response to subthreshold depolarizing current pulses (Fig. 8*A*, right). Stronger depolarizing currents evoked, in normal saline, a short-latency spike train with clear frequency adaptation (Fig. 8*B*, left). In contrast, after addition of ZD7288, the same stimulus elicited long-latency discharge, during which the spike frequency tended to increase toward the end of the pulse (Fig. 8*B*, right). Similar effects of ZD7288 as illustrated in Fig. 8*A* and *B* were observed in all five cells tested in this way. Such a slow ramp (Fig. 8*A* and *B*, right) and the much delayed discharge with 'inverse adaptation' or 'warming-up' (Fig. 8*B*, right) is typical of responses dominated by the slowly inactivating D-current (I_D) (Storm, 1988, 1990). Presumably, the effect of I_D (and also A-current, I_A) was unmasked by blockade of the opposing I_h by ZD7288 (for a discussion of this issue, see Storm, 1990, p. 179). I_D and I_A would also be strengthened by de-inactivation caused by the hyperpolarization following blockade of I_h. Accordingly, such ramp-and-delay response pattern was found to be eliminated by low concentrations of 4-aminopyridine (4-AP) or α–dendrotoxin, which block I_D (Storm, 1988, 1990; N. Gu & J. F. Storm, unpublished data).

In contrast to the ZD7288-induced reduced excitability that is illustrated in Fig. 8*A* and *B*, this blocker was also seen to increase the excitability when the cell was tested in another manner. Thus, when the ZD7288-induced hyperpolarization was eliminated by depolarizing DC, the cell produced more spikes with apparently less adaptation in response to a depolarizing current pulse than it did before ZD7288 was applied (Fig. 8*C*).

These results illustrate the mixed effects of I_h on neuronal excitability, and can be explained in the following manner. On one hand, h-channels that are open already before stimulation provide a steady inward current and depolarization that tends

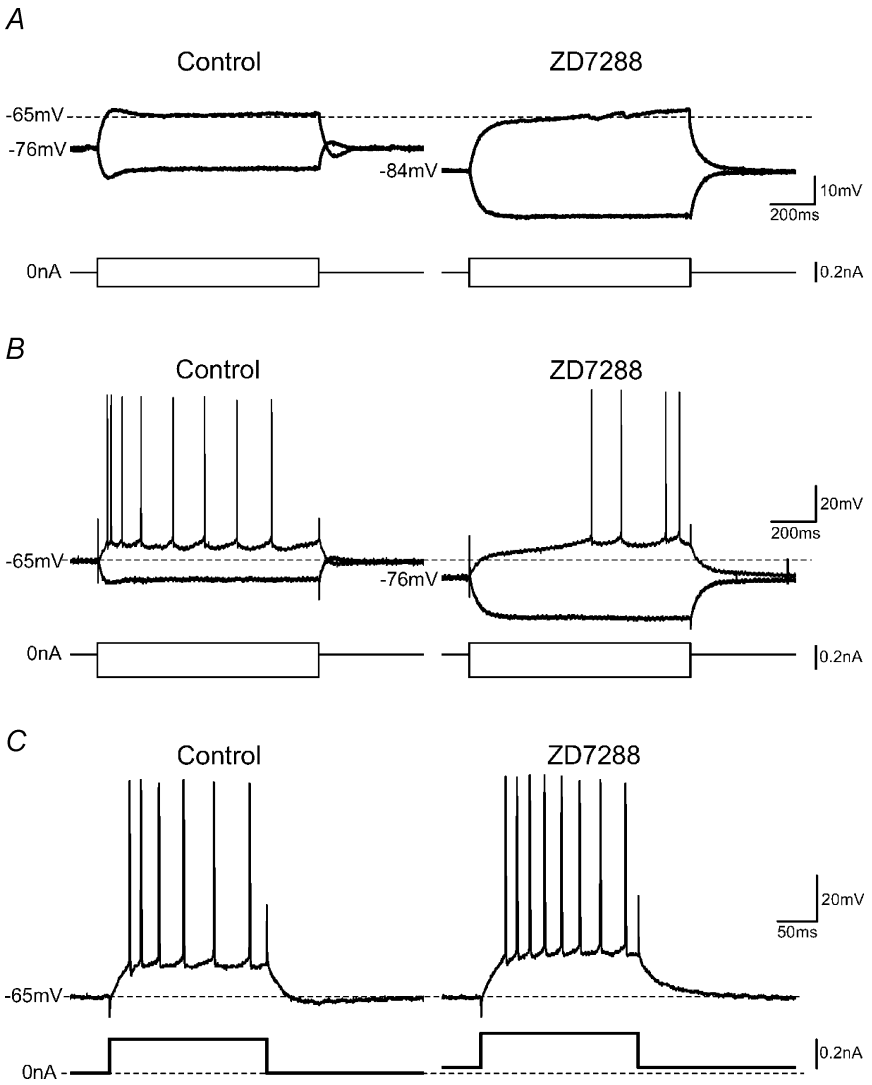

Figure 8. Complex changes in excitability resulting from I_h blockade by ZD7288
A, typical example from whole-cell recording: ZD7288 caused a hyperpolarization of V_{rest}, accompanied by an increase in the input resistance. The cell was at V_{rest} (−76 mV); current pulses (1 s duration) of opposite polarity were injected. Application of ZD7288 (10 μM) hyperpolarized the cell (in this case by 8 mV, from −76 to −84 mV), eliminated the I_h-dependent 'overshoots', 'sags' and 'rebounds' in the voltage responses; instead a slowly depolarizing ramp appeared in response to depolarizing pulses. *B* and *C*, sharp electrode recording; the cell was at V_{rest} (in this case −65 mV). Application of ZD7288 again caused a hyperpolarization, thereby reducing the excitability of the neurone, manifested as fewer APs and longer discharge latency (related to the slow depolarizing ramp shown in *A*) in response to identical current pulses (*B*). However, when the hyperpolarizing effect of ZD7288 was compensated by steady depolarizing current injection, the same cell fired more APs in response to same current pulse, indicating increased excitability (*C*), presumably due to increased input resistance, as shown in *A*. Thus, ZD7288 caused both an apparent 'increase' and an apparent 'decrease' in excitability in the same cell, depending on how it was tested. Similar effects were observed in all cells tested in this way ($n = 4$).

to increase excitability. Therefore, h-channel blockade by ZD7288 hyperpolarizes the cell and, thus, reduces its excitability (Fig. 8*B*). This inhibitory effect is further strengthened by the hyperpolarization-induced enhancement (de-inactivation) of the K^+ currents I_D and I_A, which also reduce excitability and induce a delay in the onset of firing (Fig. 8*B*, right). On the other hand, the open h-channels provide a shunt that reduces the cell input resistance. Therefore, when ZD7288 blocks these channels, the injected depolarizing current will have greater impact and produce more spikes, provided the background hyperpolarization has been compensated by DC (Fig. 8*C*, right), thus giving 'increased excitability'.

In addition, it is likely that the delayed closure of h-channels in response to depolarization, which produces the initial overshoot and sag following the onset of a subthreshold depolarization (Fig. 8*A*, left), will have a similar impact on the discharge frequency during a suprathreshold depolarization: the transient inward I_h ('overshoot') increases the frequency of the initial discharge, and the subsequent decay in I_h ('sag') contributes to the early spike frequency adaptation (Storm, 1990). This explains why the adaptation was reduced by ZD7288 (Fig. 8*C*, right). However, this effect of I_h can best be studied when the number of APs is kept constant (Fig. 9*F–I*).

Control of spike frequency adaptation

Whereas excitability reflects the overall tendency to generate APs, spike frequency adaptation specifically refers to time-dependent decline in AP frequency during a spike train. To determine the roles of I_h and I_M in early spike frequency adaptation, we evoked repetitive firing by injecting depolarizing pulses of 50–100 ms, while applying blockers of I_h and I_M (Fig. 9). In order to isolate the effect on spike frequency adaptation from effects on excitability, we kept the spike number during each pulse constant (five APs) by varying the pulse intensity. XE991 (10 μM) caused the duration of the late interspike intervals (ISIs) to be reduced relative to the first ISI, indicating a reduced adaptation (Fig 9*A* and *D*). This effect was observed in all cells tested by using both sharp electrode and whole-cell recording methods ($n = 10$) when the background V_m was -60 mV (summary data, Fig. 9*B*). At -80 mV (Fig. 9*C*), however, the effect of XE991 on the frequency towards the end of the pulse was relatively weak (Fig. 9*D*, ISIs nos 3–4), probably because of opposing effects of I_A and I_D (see above).

Since I_M activates already below the spike threshold, it may also shape subthreshold responses. To study such effects, we injected weak depolarizing current pulses and applied XE991. The pulse intensity was adjusted to be just subthreshold (Fig. 9*E*). The control response showed an initial overshoot and sag, and a small undershoot after the end of the pulse, resembling a weak mAHP (Fig. 9*E*, left, arrows), but these features disappeared after XE991 application (Fig 9*E*, right; $n = 5$). This indicates that M-channels that activate below the spike threshold can slowly shunt excitatory current, thus repolarizing the cell and reducing excitability during a maintained stimulus (Brown, 1988). When tested from a holding potential of -65 mV, XE991 application caused an increase in the cell R_{input} from 49.6 ± 6.2 to 67.1 ± 6.4 MΩ, i.e. by 38 ± 10%. (in five sharp-electrode recordings, $P = 0.009$).

To assess the role of I_h during repetitive firing, ZD7288 was applied (Fig. 9*F–I*). When the background V_m was -80 mV, ZD7288 slightly prolonged the mean duration of the first ISI (Fig. 9*H* and *I*; not statistically significant; $n = 5$, $P = 0.17$), whereas the second to fourth ISIs were significantly shortened ($P = 0.008$, 0.002, 0.002, respectively). No effect was observed when the background V_m was -60 mV (Fig. 9*F* and *G*), where h-channels are largely closed ($n = 5$, $P > 0.05$; Fig. 9*G*).

These results indicate that the inward I_h that still flows at the onset of an abrupt depolarization from a highly negative membrane potential can affect the initial excitability and spike frequency adaptation in CA1 pyramidal cells, in agreement with the data shown in Fig. 8.

The M-channel opener retigabine reduces excitability and the sAHP

In order to elucidate the functional roles of I_M, we also used the M-channel opener retigabine. Bath application of 10 μM retigabine caused a slight hyperpolarization of the cell (routinely compensated by injecting depolarizing DC: box arrows in Fig 10*A*, *C* and *E*). It also caused a clear reduction in R_{input} and increased the depolarizing overshoot and sag following a hyperpolarizing pulse (Fig. 10*C* and *D*). As expected from the hyperpolarization and reduced R_{input}, retigabine also caused a concomitant reduction in excitability, with fewer spikes evoked by a constant depolarizing current pulse (Fig. 10*E*). Furthermore, we observed a clear reduction in the amplitude of the sAHP (Fig. 10*A* and *B*, filled triangle). However, retigabine caused no significant change in the mAHP amplitude following a five-spike train at ~-60 mV (Fig. 10*A*, *B* and *F*; $n = 4$, $P > 0.05$). All effects of retigabine were reversed by XE991, as expected (Fig. 10*A–E*).

We interpret these results as follows. At depolarized potentials (~-60 mV) the M-channels are slightly activated, thus providing a small standing outward current and shunt that tends to hyperpolarize the cell and reduces the cell R_{input}. Retigabine, which shifts the activation curve of I_M to more negative levels (Tatulian *et al.* 2001), thus increases M-channel activation at ~-60 mV, enhancing the shunt (reducing R_{input}; Fig. 10*C*)

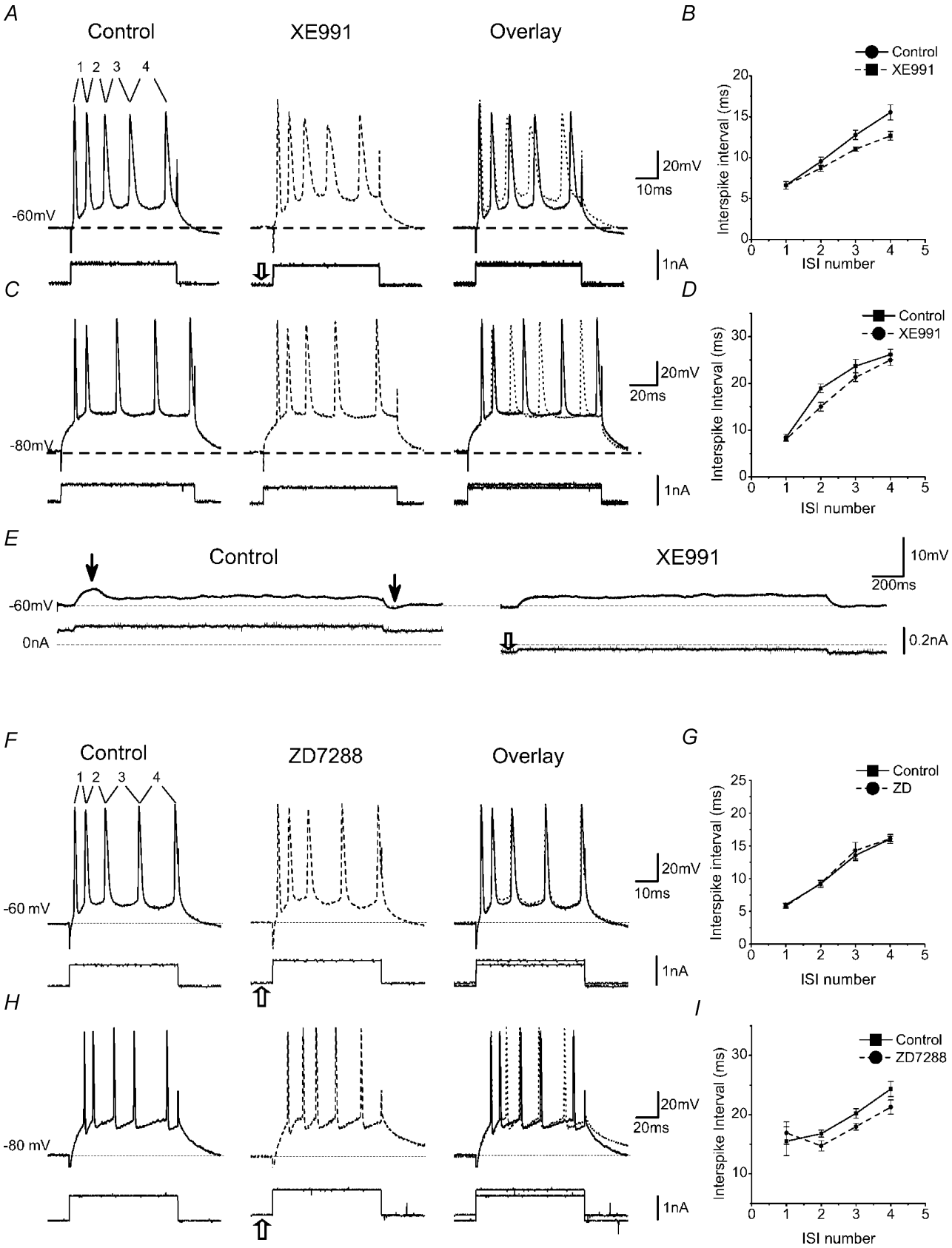

as well as the I_M-dependent sag (after the overshoot in Fig. 10*C*, middle trace), and hyperpolarizing the cell (compensated by DC in Fig. 10*A*–*C*, box arrows). The retigabine-induced reduction in R_{input} reduces the effect of injected depolarizing current, thus reducing the number of APs evoked by a given current intensity (Fig. 10*E*). The diminished R_{input} also reduces the impact of natural hyperpolarizing currents, such as the sAHP-current evoked by five spikes, thus reducing the amplitude of the sAHP (Fig. 10*A*(filled triangle) and 10*B*). The possibility that the reduction in the sAHP may be due to a partial block of Na^+ channels, and shift in Ca^{2+} channel activation by 10 μM retigabine (Rundfeldt & Netzer, 2000), seems unlikely because the effect of retigabine on the sAHP amplitude was largely reversed when I_M was blocked by adding XE991, although retigabine was still present (Fig. 10*B*). Besides, computational simulations of the retigabine effect on I_M showed that the sAHP reduction can readily be explained as a consequence of the specific changes in the M-conductance (see below; Figs 11*B* and 12*B*). Therefore, the change in the sAHP (Fig. 10*A*–*B*) was probably a direct consequence of I_M enhancement, rather than a nonspecific effect.

The observation that the mAHP amplitude was not significantly altered by retigabine (Fig. 10*A*(open triangle), *B* and *F*) or even slightly reduced (Fig. 10*A*–*B*), may be explained by considering several opposing effects. Retigabine shifts the steady-state activation curve of I_M to more hyperpolarized potentials (Tatulian *et al.* 2001). Therefore, at −60 mV, there is a larger standing I_M, implying that there will be less I_M relaxation after a spike or spike train. For example, if the M-channels – in the extreme – were fully opened at −60 mV, then spikes could cause no further I_M activation and, hence, no mAHP at all at this potential. On the other hand, if retigabine also causes a hyperpolarizing shift in the activation and deactivation kinetics of I_M, its activation during the spike might speed up, causing more I_M activation and, thus, a larger mAHP amplitude. These effects are further illustrated by computational modelling in Figs 11*B*1 and 12*B*1 (insets).

Computational analysis of the mAHP mechanisms following a single AP

Although the above experiments with selective channel blockers can elucidate qualitative questions about which ion channels contribute to the mAHP, they do not answer a number of important quantitative questions that may be hard to handle intuitively. For example: how can I_M, in spite of its overall very slow kinetics, activate sufficiently during a single AP to account for the observed mAHP (Fig. 6)?

In order to examine issues like these, we performed a computational analysis of the mAHP mechanisms, using a similar mathematical model of a CA1 pyramidal cell that was used previously in our laboratory (Hu *et al.* 2002*b*; Shao *et al.* 1999; for details, see Methods, and Supplemental material for computer modelling).

Figure 11*A* shows (at two different time scales) that a simulated single AP evoked by a brief (1 ms) current pulse, gave rise to a fAHP (largely due to BK current), mAHP (largely due to I_M) and sAHP (largely due to I_{sAHP}). A constant current injection was used to keep the background V_m at −60 mV, as in the slice experiments. When the sAHP current was omitted, the mAHP peak amplitude decreased slightly (dash-dot-dot traces; open triangle), resembling the effect of forskolin-induced suppression of I_{sAHP} (Fig. 2*B*1). This illustrates that the early I_{sAHP}, due to overlap, can contribute to the early AHP amplitude at the peak of the mAHP.

In Fig. 11*B*1, single APs were evoked while changing the background V_m from −60 to −80 mV, with no currents blocked (continuous line). The results show how hyperpolarization reduced the fAHP and mAHP due to a reduced driving force. Subsequently, the simulations were

Figure 9. I_M and I_h regulate early spike frequency adaptation in a voltage-dependent manner
A–*D*, XE991 (10 μM) reduced the early spike frequency adaptation, at background membrane potentials of −60 mV (*A* and *B*) and −80 mV (*C* and *D*). The cell was kept either at −60 mV (*A*) or at −80 mV (*C*) by steady current injection. A depolarizing current pulse lasting 50 (*A*) or 100 ms (*C*) was injected every 20 s to evoke constant number (5) of APs. At −80 mV (*C*), 100 ms pulse duration was used, because 50 ms was often insufficient for evoking five APs. The first to the fourth interspike intervals (ISIs) were compared before and after each drug application. *B* and *D*, summary data of spike frequency adaptation before and after XE991 at −60 mV (*B*) and at −80 mV (*D*). Note that XE991 inhibited early spike frequency adaptation at −60 mV, manifested as reduction of the second to fourth ISIs. However, at −80 mV, XE991 only significantly reduced the second and third ISIs. *E*, typical responses to subthreshold depolarizing current pulse injection (1 s duration) before and after XE991 application. The overshoot (↓) and sag in the control condition was inhibited by XE991. In order to obtain responses of comparable, subthreshold amplitudes, the current pulse amplitude was reduced to compensate for the increased input resistance induced by XE991, and the XE991-induced depolarization was compensated by reducing the positive holding current (open arrow). *F*–*I*, typical examples showing the effect of ZD7288 on early spike frequency adaptation at −60 mV (*F*–*G*) and −80 mV (*H*–*I*). Note that ZD7288 reduced early spike frequency adaptation only when spikes were evoked from −80 mV, reflected as changes in the second to fourth ISIs (summary data in *G* and *I*). *A*, whole-cell recording; *C*, *E*, *F* and *H*, sharp electrode intracellular recordings.

repeated after eliminating some of the ionic currents. When I_M was omitted (dashed line), the mAHP was virtually abolished at −60 mV, while there was no effect at −80 mV, thus resembling the results with XE991 (cf. Figs 2 and 4). In contrast, when I_h was omitted (dash-dot line), the mAHP was abolished at −80 mV (Fig. 11*B*1, right) but not affected at −60 mV, thus mimicking the effects of ZD7288 (cf. Fig. 5*A*–*D*).

The inset of Fig. 11*B*1 compares the sAHP under normal conditions (continuous line) and when I_M was blocked (dashed line) or enhanced by shifting its voltage-dependence (thin dotted line). The increased sAHP amplitude following elimination of I_M (dashed line) was simply due to the increased R_{input}, caused by lack of M-conductance. This largely explains the experimentally observed effects of XE991 (increased sAHP; in Fig. 4*A*) and retigabine (reduced sAHP due to increased M-conductance that reduces R_{input}; in Fig. 10*A*). Blocking I_M also caused a slight depolarization of the membrane potential as in the experiments at −60 mV. Also, we simulated the retigabine effect by shifting the I_M steady-state activation curve by −7 mV (Tatulian *et al.* 2001) (inset of Fig. 11*B*1, thin dotted line). This caused a strong reduction in the sAHP (through a decrease in R_{input}) and a slight decrease of the mAHP, thus resembling qualitatively the experimental observations of Fig. 10*A* and

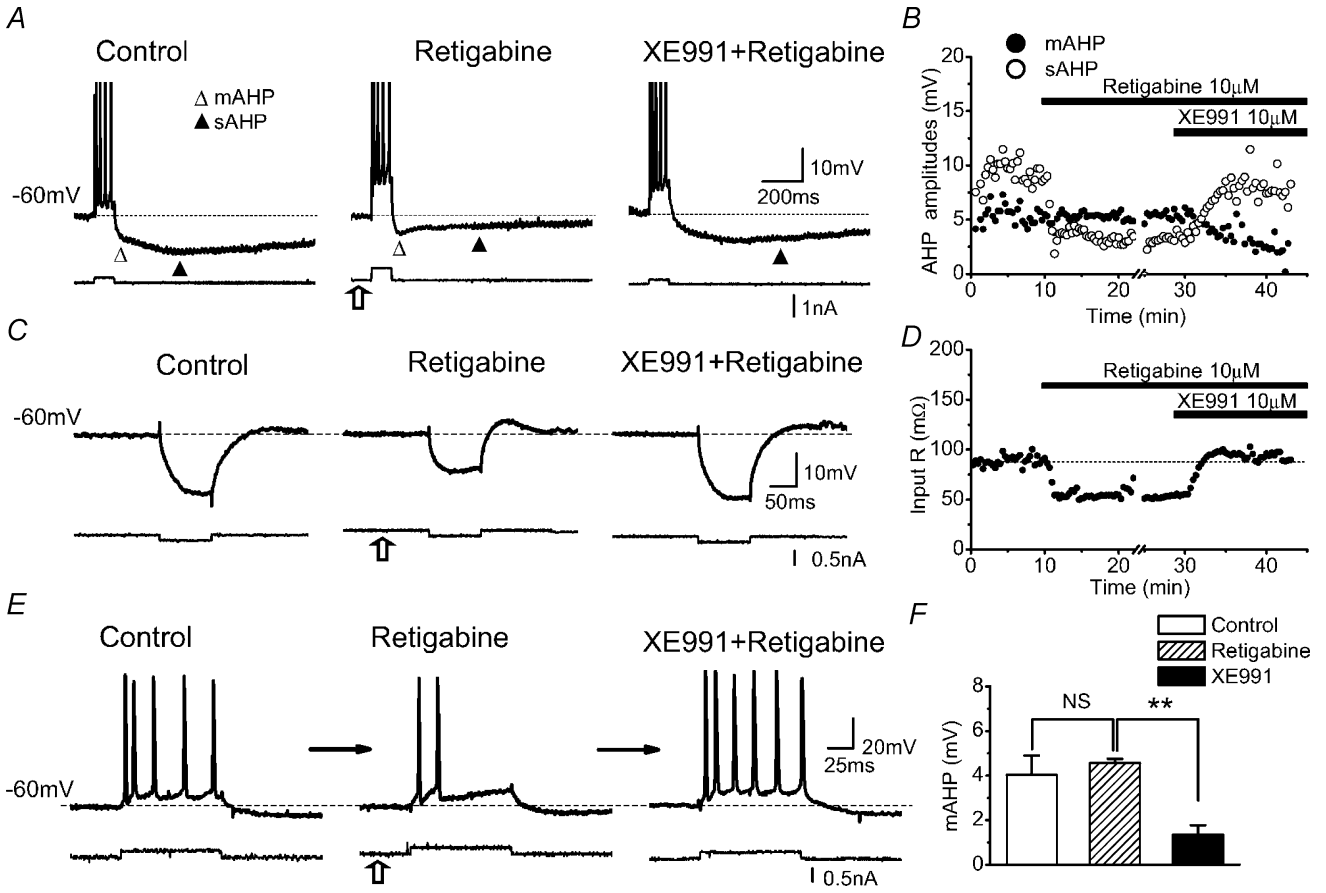

Figure 10. The effect of the Kv7/KCNQ/M-channel opener retigabine on the mAHP, early spike frequency adaptation and input resistance

A and *B*, mAHP (△) and sAHP (▲) following a train of five spikes, recorded under normal conditions, followed by application of 10 μM retigabine and subsequently 10 μM XE991. Retigabine caused the cell to hyperpolarize, but this was reversed by increasing the positive steady current to keep the membrane potential at −60 mV (open arrow). However, retigabine had no apparent effect on the mAHP, whereas the sAHP was reduced by ∼50%. XE991 blocked the mAHP and fully reversed the effect of retigabine on the sAHP and membrane potential. *B*, time courses of the mAHP (●) and sAHP (○) amplitudes during the experiment illustrated in *A*. *C* and *D*, retigabine reduced the input resistance at −60 mV by 38.9 ± 3.1% (mean ± S.E.M.), and increased the rebound; both effects were blocked by XE991 (same cell as in *A* and *B*). *E*, retigabine reduced the excitability of the cell, reflected as fewer APs evoked by a current pulse of constant amplitude. The open arrows in *A*, *C* and *E* indicate that less positive steady current was injected into the neurone after retigabine to keep it at −60 mV, reflecting that retigabine had a hyperpolarizing effect. *F*, summary data showing the effect of retigabine and XE991 on the mAHP amplitude ($n = 4$, NS $P > 0.05$, $^{**}P < 0.01$). All cells were obtained with sharp electrode recording.

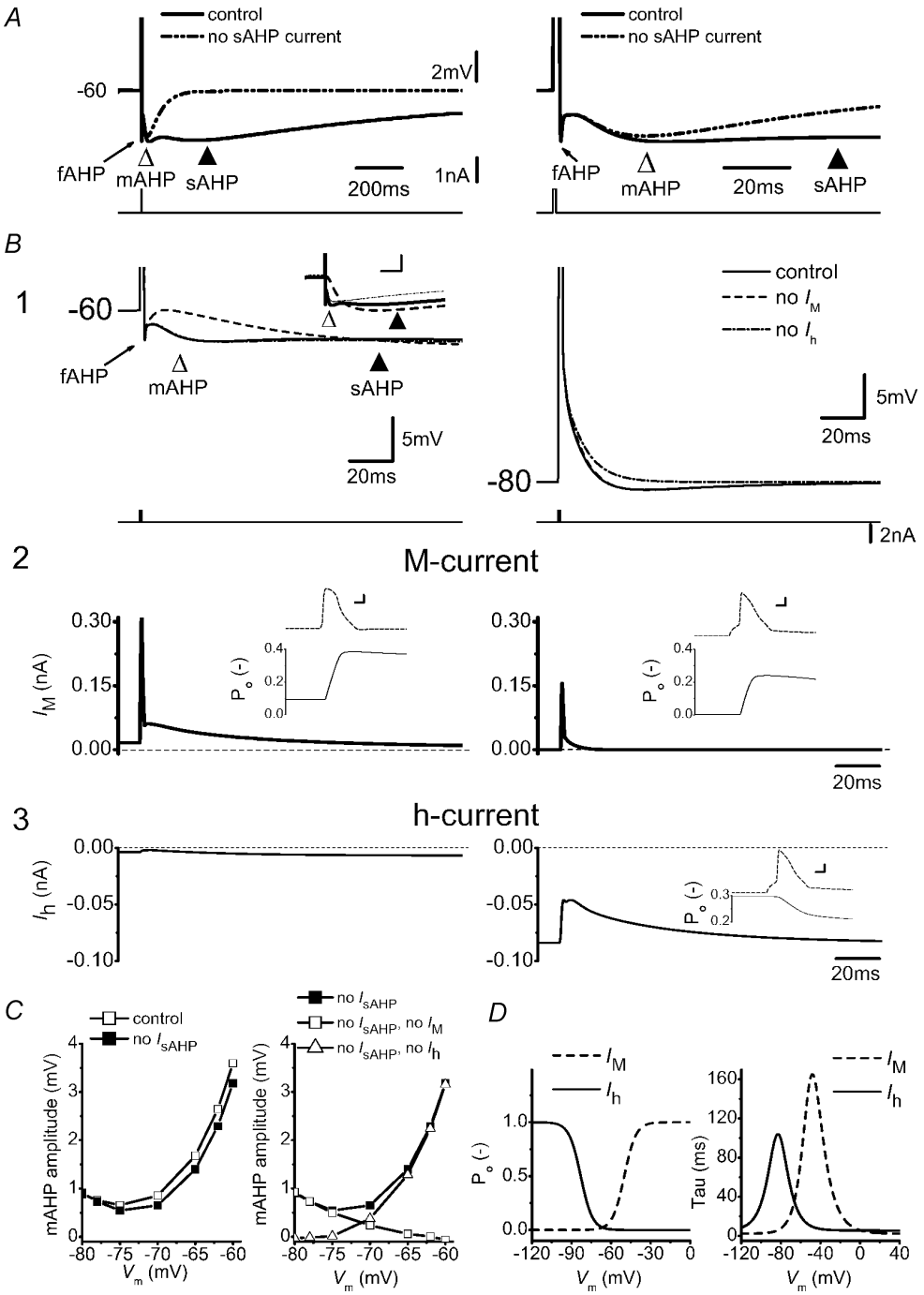

Figure 11. Modelling study of the mAHP following a single AP
A, a single AP evoked by a current pulse (1 ms) while holding the membrane potential at −60 mV by steady-state current. Simulations were repeated with and without sAHP current. The left- and right-hand panels show the same simulations at different time scales. *B*1, same protocol as *A* while holding the membrane potential at different levels, as indicated. Superimposed voltage responses of simulations are shown of 'control' or with either 'no I_M' or 'no I_h'. *B*1, inset, (at a different scale) the AHPs following a single spike evoked at −60 mV, in normal conditions (control, continuous line), without I_M ('no I_M', dashed line) and with a −7 mV negative shift of the I_M steady-state activation curve, i.e. resembling the retigabine effect (thin dotted line). Note that blocking I_M or shifting its activation curve towards more negative potentials, increases and decreases the sAHP, respectively. *B*2 and *B*3, I_M and I_h responses, respectively, during the protocol shown in *B*1. Insets show the open probability (P_o) of I_M (*B*2) or I_h (*B*3) during the AP. *C*, left panel, summary data of the mAHP amplitude at various holding potentials with or without sAHP current. Right panel, voltage dependence of the amplitude of the isolated mAHP (i.e. without sAHP current) with either I_M or I_h blocked. *D*, voltage dependence of the P_o (left) and time constant (right) of I_M and I_h. Scale bar of insets in *B*1: 100 ms, 2 mV; *B*2 and *B*3: 0.5 ms, 20 mV.

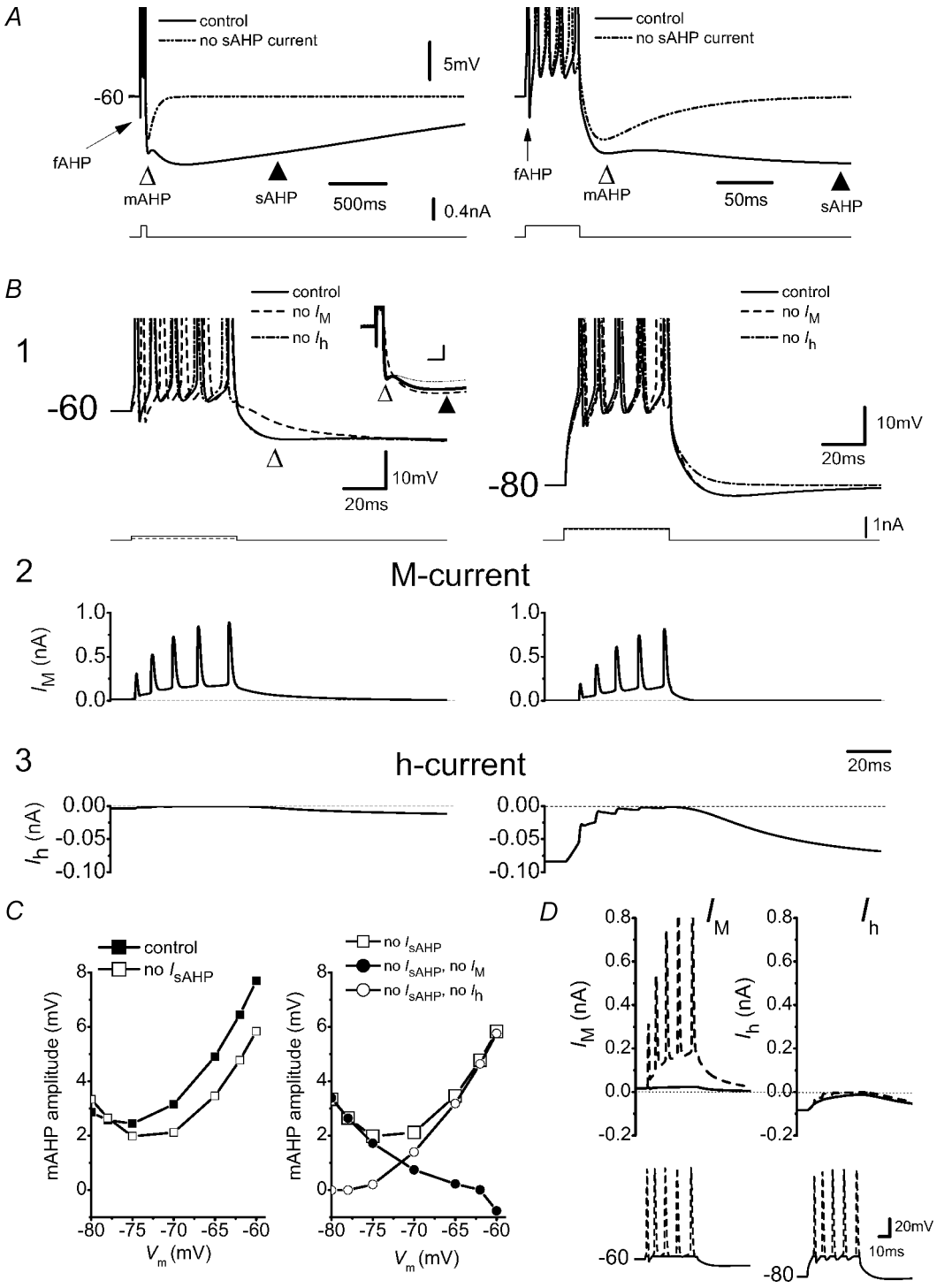

Figure 12. Modelling study of the mAHP following a train of APs

A, train of APs evoked by a current pulse (50 ms) while holding the membrane potential at −60 mV by steady-state current. Simulations were repeated with and without sAHP current. The left- and right-hand panels show the same simulations at different time scales. *B*1, same protocol as *A* while holding the membrane potential at different levels as indicated. Voltage responses of simulations of normal conditions or with either 'no I_M' or 'no I_h' are shown superimposed. The inset in *B*1 shows the AHPs following a five-spike train evoked at −60 mV, in normal conditions (control, continuous line), without I_M ('no I_M', dashed line) and with a −7 mV negative shift of the I_M steady-state activation curve, i.e. resembling the retigabine effect (thin dotted line). Note that blocking I_M, or shifting its activation curve, increases and decreases the sAHP, respectively. *B*2 and *B*3, I_M and I_h response,

B. The simulated retigabine effect also caused a hyperpolarization of V_m at −60 mV. These simulations show that the observed effects of XE991 and retigabine can be explained in terms of their specific actions on I_M, thus not implying any side effects.

The lower two panels (Fig. 11*B*2–3) show the currents underlying the mAHP: I_M and I_h. The insets show the open probabilities (P_o) of the M-channels (Fig. 11*B*2) and h-channels (Fig. 11*B*3) during the AP, at a fast time scale. Due to their slow kinetics, the M-channels open late during the AP (Fig. 11*B*2). Thus, only about 30% of the full M-conductance ($g_M = 7\ pS\ \mu M^{-2}$) is activated by a single spike in the model. I_M increases from ∼10% (P_o ∼0.10) to ∼40% (P_o ∼0.40) activation (inset of panel Fig. 11*B*2, left). However, this is sufficient to account for the observed single-AP mAHP amplitude of 2–5 mV at ∼−60 mV (compare Figs 6*A* and 11*A*) (Storm, 1989). In contrast to I_M, I_h showed little change during the AP, partly because of the slowness of I_h. When starting from −80 mV, where I_h is moderately activated, I_h is very small during the AP itself because of its reduced driving force at depolarized potentials (Fig. 11*B*3, right). Nevertheless, starting from −80 mV, I_h is sufficiently deactivated by a single AP and ADP (∼70% of the deactivation was due to the AP and ∼30% due to the ADP) to generate a very small mAHP at that potential (Fig. 11*B*1 and 3). This is in agreement with the slice experiments (Fig. 5; see also Storm, 1989).

Figure 11*C* (left panel) summarizes the voltage dependence of the mAHP after a single AP, with or without the sAHP current included in the model. The right panel shows the changes in mAHP amplitude when various currents are blocked: (filled squares, no I_{sAHP}; open squares, no I_{sAHP} and no I_M; open triangles, no I_{sAHP} and no I_h). Figure 11*D* shows the voltage dependence of the open probabilities and time constants of the M- and h-channels used in the model. In accordance with the consistently negative experimental results with Ca^{2+}-free medium or SK-channel blockers (Figs 1*A*, 2, 3*C* and *D*, and 7*D*–*F*), no SK conductance was included in the model.

Computational analysis of the mAHP following a train of APs

Figure 12*A* (upper traces) shows a simulated train of five spikes at two different time scales. The train was evoked by a 50 ms current pulse, while the background V_m was maintained at −60 mV with constant current injection (i.e. similar to the wet experiments shown in Fig. 4*A*). Elimination of I_{sAHP} (dash-dot-dot traces) caused a small reduction in the mAHP amplitude, similar to the forskolin effect in Fig. 2*B* (open triangle).

Figure 12*B* shows the effects of changing the background V_m in the normal model (i.e. with all currents included) and after omitting I_M or I_h. Again, the mAHP is shown to be due to I_M at −60 mV, but is caused by I_h at −80 mV (Storm, 1989).

The lower panels (Fig. 12*B*2 and 3) show ionic currents during the spike trains at −60 and −80 mV. Again (cf. Figure 11*B*2 and 3), I_M is activated during each AP, but also during the ISIs, and is the main current during the postburst mAHP at −60 mV. It participates appreciably to the mAHP also at −70 mV (data not shown). In contrast, I_h was small during each AP (Fig. 12*B*3), but deactivates substantially during the 50 ms depolarization, thus generating the mAHP at −80 mV, in agreement with our experimental results (Fig. 5). Figure 12*C* shows the voltage dependence of the mAHP after five APs, with and without I_{sAHP}, I_M and/or I_h. These plots illustrate the graded transition from an I_M-dependent mAHP at depolarized potentials to an I_h-dependent mAHP at hyperpolarized potentials, resulting in an overall U-shaped voltage dependence of the mAHP amplitude (Figs 11*C* and 12*C*) (Williamson & Alger, 1990).

Given the very slow kinetics of I_M and I_h, it may seem surprising that they can be significantly affected by APs. To test whether I_M and I_h are activated by the APs themselves, or by the subthreshold 'envelope' depolarization caused by the injected current pulse, we compared the currents evoked by the full voltage response of the model cell, including the spike train (Fig. 12*D*, dashed lines), with the same voltage response without the spikes, i.e. each AP was cut off at the spike threshold (Fig. 12*D*, continuous lines). These voltage responses, which were used as voltage clamp commands in the model (lower panels in Fig. 12*D*), were based on the current-clamp simulations as shown in Fig. 12*A* (a 50 ms pulse evoking five APs), either at −60 mV (Fig. 12*D*, left) or at −80 mV (right). As shown in the upper panels in Fig. 12*D*, I_M was predominantly activated during the spikes (left), whereas

respectively, during the protocol shown in *B*1. *C*, left panel, summary data of the mAHP amplitude at various holding potentials with or without sAHP current. Right panel, voltage dependence of the amplitude of the isolated mAHP (i.e. without sAHP current) with either I_M or I_h blocked. *D*, to determine whether I_M and I_h are activated and deactivated, respectively, by the APs or by the interspike depolarized plateau during a spike train (as in *B*), we compared I_M and I_h during voltage responses with and without spikes. The voltage responses from the simulations in *B*1 at −60 and −80 mV, with or without spikes, were used as voltage-clamp commands (lower panels, dashed traces and continuous lines, respectively). The APs were clipped at the threshold. Upper panels, I_M (left) and I_h (right) during the voltage-clamp command, before (dashed traces) and after (continuous lines) clipping the APs. Note that I_M was strongly reduced by eliminating the spikes, indicating that it was mainly activated during the APs. In contrast, I_h was little affected by clipping the spikes, showing that it was mainly activated by the depolarized plateau. Inset scale bar of *B*1: 100 ms, 2 mV.

I_h was almost identical with and without spikes (right), i.e. I_h was mainly deactivated by the subthreshold 'envelope' depolarization.

This issue was also explored experimentally (Fig. S1). Varying the number of spikes from 0 to 9 during a current-pulse-induced depolarization (200 ms) from −80 mV had virtually no effect on the ensuing mAHP (Fig. S1*A* and *B*). Furthermore, blocking the spikes with TTX had no detectable effect on the mAHP following a depolarizing pulse (200 ms; 5–10 spikes) at −80 mV ($n = 4$, $P > 0.05$; Fig. S1*C* and *D*), in good agreement with our modelling results (Fig. 12*D*).

Spike frequency adaptation in the model

Finally, we studied the adaptation during a spike train with the model (Fig. 13) by using a stimulation protocol similar to the one used in the slice experiments (see Fig. 9). Figure 13*A* shows that elimination of I_M reduced the spike frequency adaptation during a pulse-evoked train of five APs, both when the background V_m was −60 mV (left panels) and when it was −80 mV (right). In contrast, blockade of I_h affected only the initial AP frequency evoked from −80 mV (Fig. 13*B*), because the h-channels close during maintained depolarization.

To compare the overall degree of adaptation during the five-spike trains, we fitted a straight line to each of the plots in Fig. 9*B*, *D*, *G* and *I*, and Fig. 13*A* and *B*, and compared the slope (called adaptation index) of these linear fits (Fig. 13*C* and *D*). For each condition we found an overall qualitative agreement between the model and experiments. Thus, at a background membrane potential of −60 mV, both the experiments and the simulations showed that elimination of I_M reduced the adaptation index, whereas elimination of I_h had essentially no effect on this parameter (Fig. 13*C*). In contrast,

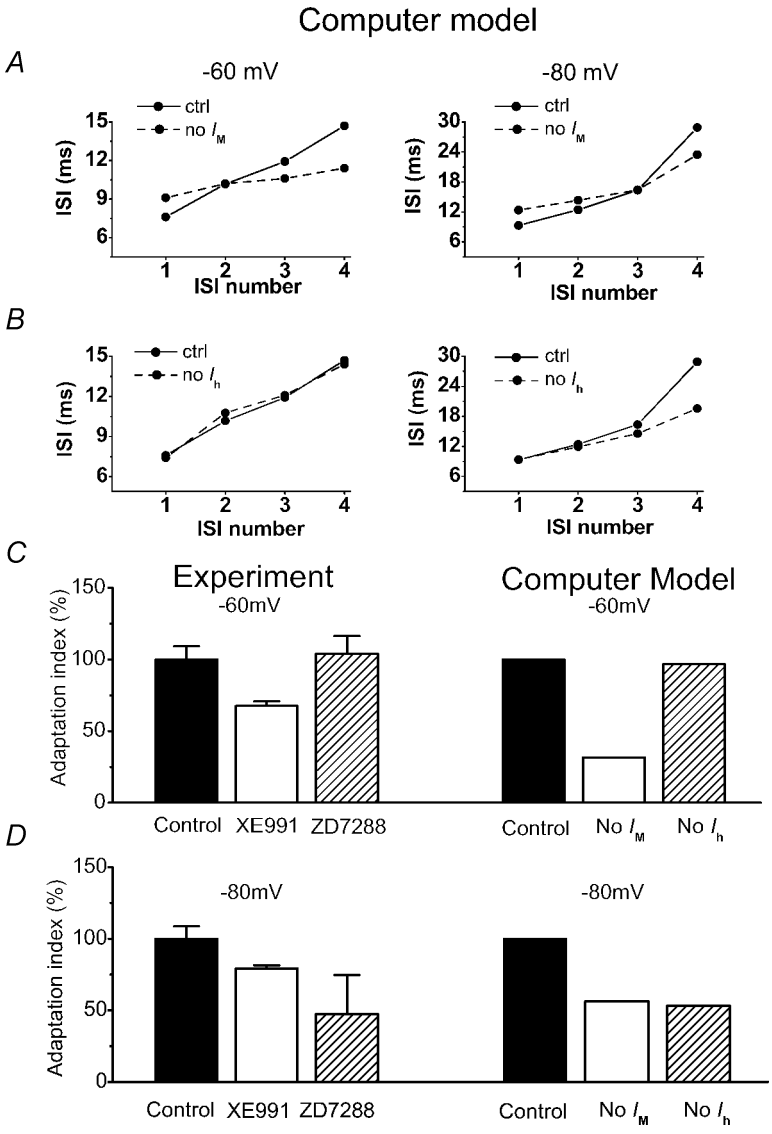

Figure 13. Contributions of I_M and I_h to spike frequency adaptation during repetitive firing: comparing experimental and modelling results
By using the same computer model as in Figs 11 and 12, a train of five APs was evoked by a 50 ms current pulse. The first to the fourth ISIs were compared with and without I_M (*A*) and I_h (*B*) while holding the cell at −60 mV (left) and −80 mV (right). *C* and *D*, bars show the normalized adaptation index from experiment data (left) compared with the results from the modelling study (right), at background membrane potentials of −60 (*C*) and −80 mV (*D*). The adaptation index was defined as the slope of the line that fitted best to the plot of the four ISIs (first to fourth ISIs), as shown in *A* and *B*. In both the experiments and the modelling, we consistently found at −60 mV that elimination of I_M reduced the adaptation index, whereas elimination of I_h had little effect. In contrast, at −80 mV, elimination of either I_M or I_h significantly reduced the adaptation index.

at −80 mV, elimination of I_M or I_h each reduced the adaptation, both in the experiments and in the model (Fig. 13*D*).

However, in both the model and the slice experiments, it was hard to control the precise timing of the last spike in the train. Consequently, the instantaneous frequencies were inevitably somewhat variable. It is therefore perhaps not surprising that there are some quantitative differences in the details of the adaptation both within the experimental data and between them and the simulation results (compare Fig. 9 with Fig. 13*A* and *B*), and it does not appear fruitful at this stage to further explore these differences in detail. We also chose not to tune our model to the details of our experimental data on spike frequency adaptation, since that would either mask the limitations of our model at this stage, or else require a thorough experimental exploration of related issues that was not the primary aim of this study, e.g. the relative contributions of various K^+ channels to spike repolarization at different background membrane potentials.

Discussion

The main conclusions of this study are that the somatic medium afterhyperpolarization – mAHP – in rat CA1 hippocampal pyramidal cells is generated mainly by Kv7/KCNQ/M-channels at depolarized membrane potentials, and by HCN/h-channels at hyperpolarized membrane potentials, with little or no contribution from SK ($K_{Ca}2$) type Ca^{2+}-activated K^+ channels at either potential. These conclusions seem to hold both for the mAHP following a single AP and for the mAHP that follows a spike burst.

The role of SK channels

We found no evidence for a contribution of SK channels or other Ca^{2+}-activated K^+ channels to the mAHP (Figs 1–3). Furthermore, no contribution of SK channels to spike frequency adaptation or excitability control could be detected (Fig. 7*D–H*). These results may be regarded as surprising in view of the evidence and prevailing idea that generation of afterhyperpolarizations, frequency adaptation and excitability control are the main functions of SK channels in neurones in general and CA1 pyramidal cells in particular (Kohler *et al.* 1996; Norris *et al.* 1998; Stocker *et al.* 1999; Bond *et al.* 1999; Hille, 2001; Stackman *et al.* 2002; Sah & Faber, 2002; Sailer *et al.* 2002; Melyan *et al.* 2002; Faber & Sah, 2003; Wittekindt *et al.* 2004). Our results are unexpected also because functional SK channels evidently are expressed in the somatodendritic membrane of CA1 pyramidal cells and can generate a robust outward current (Sailer *et al.* 2002), and because normal APs in these cells cause a sufficient rise in intracellular Ca^{2+} concentration to readily activate two other classes of Ca^{2+}-activated K^+ channels: the BK channels, and the sAHP channels (Storm, 1987*a*, 1990; Lancaster & Nicoll, 1987).

However, our conclusion is in good agreement with the recent finding that SK-channel blockade by apamin, unlike M-channel blockade, fails to facilitate the ADP in these cells (Yue & Yaari, 2004). Our conclusion is also fully compatible with the recent finding of Villalobos *et al.* (2004) that overexpression of SK1 or SK2 subunits in mice enhanced the mAHP in neocortical pyramidal cells. Thus, our results from CA1 pyramidal cells obviously do not preclude that SK channels can generate mAHPs in other types on neurones (Schwindt *et al.* 1988; Abel *et al.* 2004). On the contrary, we have recently found that bursting pyramidal cells in the rat subiculum generate a prominent SK mAHP that is substantially reduced by SK-channel blockers (Hu *et al.* 2004), and we have detected SK mAHPs also in rat neocortical pyramidal cells (H. Hu & J. F. Storm, unpublished; Foehring *et al.* 1989; Abel *et al.* 2004) and cerebellar Purkinje cells (H. Hu & J. F. Storm, unpublished; Cingolani *et al.* 2002). We do not know why others have observed apparent reductions in mAHP amplitude and increased excitability after apamin application in CA1 pyramidal cells (Stocker *et al.* 1999; Stackman *et al.* 2002). However, the lack of time course plots for the apamin effects in those articles, seem to leave open the possibility that a gradual drug-independent run-down of I_M and the mAHP during the whole-cell recordings might have been mistaken for an effect of apamin.

If SK channels do not contribute to the somatic mAHP, then what is their function in CA1 pyramidal neurones? An important hint is given in a recent report by Cai *et al.* (2004) who conclude that SK channels contribute to the repolarization of Ca^{2+}-mediated plateau potentials in thin oblique dendrites of these neurones, indicating a prominent role in dendritic integration.

The role of the M-channels

The conclusion that I_M is the main mechanism of the mAHP at depolarized membrane potentials was already reached 15 years ago (Storm, 1987*b*, 1989) and was soon confirmed (Williamson & Alger, 1990). However, both of these studies relied on the nonspecific pharmacological agents for I_M suppression that were available at that time: Ba^{2+} ions, TEA and muscarinic agonists (Halliwell & Adams, 1982; Madison *et al.* 1987; Storm, 1989). It is therefore reassuring to find the main conclusion from that time being confirmed, in particular by use of the highly specific M-channel blocker XE991 (Wang *et al.* 1998), which fully suppressed the mAHP at depolarized membrane potentials, whereas blockade of SK channels failed to suppress the mAHP.

However, it may seem surprising or even dubious (Lancaster & Pennefather, 1987; Yue & Yaari, 2004) that the M-channels, given their overall very slow activation kinetics with time constants in the 100 ms range, can activate appreciably during a single AP that lasts only 1–2 ms, thus generating quite prominent single-spike mAHPs (Storm, 1989). Hence, it has been suggested that the M-channels actually open during the ADP that follow the spike, rather than during the AP itself (Yue & Yaari, 2004). However, the latter hypothesis hardly explains how M-channels can generate the single-spike mAHPs in depolarized cells or during slow repetitive firing (Fig. 6*A*; see also Lanthorn *et al.* 1984; Storm, 1989), since there is little or no ADP under those conditions. Unfortunately, there is a lack of data on native I_M kinetics in mammalian neurones at depolarized potentials beyond −20 mV (Wang *et al.* 1998). In our computational model, we used a plausible extension of the somatic I_M kinetics with a strong voltage dependence of the I_M time constant, which implies a much faster activation beyond −20 mV. Previous data have shown a strong voltage dependence of I_M deactivation (Halliwell & Adams, 1982; Wang *et al.* 1998), but there is little data on the activation time constants. Moreover, both I_M and I_h kinetics were reported to be very temperature sensitive (Halliwell & Adams, 1982; Magee, 1998). Both currents show a Q_{10} close to 5.0. Hence, the I_M-mediated mAHP might be even more prominent at physiological temperatures due to faster activation, although both the spikes and the resulting mAHP would be of shorter duration. To exclude other possible explanations than a fast time constant at depolarized potentials, we constrained the parameter space of our model by fitting it to the voltage clamp data of I_h, I_M and I_{NaP} that were obtained in our previous study (Hu *et al.* 2002*b*).

In our model, I_M activates by ∼30% ($g_M = 7$ pS μm^{-2}) during a single spike (Fig. 11*B*2), thus producing mAHPs that closely resemble those obtained experimentally. This is in good agreement with previous estimates (Storm, 1987*a*, 1989) and recent evidence that KCNQ2 channels in axons can activate during single APs (Devaux *et al.* 2004). Thus, the reason why I_M has only a negligible contribution to the repolarization of a single spike (Storm, 1989; Yue & Yaari, 2004) is probably not that it fails to activate during the spike, but that the activated I_M is far smaller than the main repolarizing Kv and BK currents (Storm, 1987*a*, 1989, 1990). In contrast, once the Kv and BK channels have closed following AP repolarization and the fAHP, I_M for a while becomes the dominating current, thus generating the mAHP (Fig. 11*B*2; Storm, 1989).

The role of the HCN/h-channels

That I_h (HCN current, previously called I_Q; Halliwell & Adams, 1982) is the main generator of the mAHP at hyperpolarized membrane potentials but not at depolarized potentials was also concluded previously (Storm, 1989, 1990) and confirmed by Williamson & Alger (1990). However, since this conclusion was to a large extent based on results with the nonspecific blocker Cs^+ – the best I_h blocker available at the time (Halliwell & Adams, 1982) – it is reassuring that extensive tests with the far more specific h-channel blocker ZD7288 led to the same conclusions (Fig. 5). In particular, the previous suggestion that the mAHP in rat CA1 pyramidal cell is caused exclusively by I_h, with essentially no contribution from other currents (Maccaferri *et al.* 1993) is contradicted by our results with I_M blockers, and by the fact that we detected no I_h contribution to the prominent postburst mAHP at depolarized potentials, including the functionally important single-spike mAHPs during slow repetitive firing (Fig. 6). A possible explanation for the different conclusions reached by Maccaferri *et al.* (1993) and us (Storm, 1989), is that they used slices from very young rats (14–18 days), in which I_M may not be well developed.

Comparison between M-mAHP and H-mAHP

Another conclusion is that I_M and I_h produce mAHPs in very different ways. In analogy with the M-resonance and H-resonance described in these cells (Hu *et al.* 2002*b*), we suggest the terms 'M-mAHP' and 'H-mAHP' to distinguish the two forms of mAHP. I_M is activated primarily by the APs (Fig. 12*D*; see also Fig. 10 in Storm, 1989), thus producing a slow outward tail current that outlasts the spike and generates the M-mAHP. The M-mAHP can inhibit subsequent spiking, both through its hyperpolarization and through the reduced R_{input} ('shunting') it provides. Thus the M-mAHP – i.e. the I_M-dependent mAHP – is a real spike-afterpotential, and provides a genuine negative *feedback* control of excitability (Storm, 1989). In contrast, I_h generates the H-mAHP at highly negative potentials, by turning *off* (i.e. h-channels that were open before the stimulus are closed by the depolarization) rather than by turning on (Fig. 11*B*3). Furthermore, the resulting 'outward' tail current (i.e. reduction in inward I_h) that underlies the H-mAHP is no real *spike*-afterpotential, because it is mainly caused by the *subthreshold* depolarization provided by depolarizing current injection or EPSPs, rather than by the spikes (Fig. 12*D* and Fig. S1; see also Fig. 10 in Storm, 1989). Thus, although pacemaker potentials and mAHPs may seem to be quite different phenomena, the roles of I_h, in pacemaking in the cardiac AV node (DiFrancesco, 1995) or in thalamic relay cells in bursting mode (McCormick & Huguenard, 1992) on one hand, and in the hippocampal mAHPs on the other, are quite analogous. In both cases, I_h is deactivated by a long-lasting depolarization (provided by

the cardiac AP (DiFrancesco, 1986), a T-channel-induced burst in thalamic cells (Pape, 1996; Luthi & McCormick, 1999), or a depolarizing pulse or train of EPSPs in CA1 cells), thus causing a hyperpolarization that postpones subsequent APs until I_h has slowly activated again. Hence, the cardiac pacemaker potential is analogous to the decay of the hippocampal H-mAHP.

The mAHP amplitude showed a U-shaped voltage-dependence (Figs 11*C* and 12*C*; see also Williamson & Alger, 1990). Thus, at V_{rest} (which varies from about −65 to −75 mV in these cells, the exact value depending on the recording conditions), the mAHP amplitude is relatively small compared to mAHPs at more depolarized or hyperpolarized potentials (Figs 11*C* and 12*C*). As indicated by this analysis, the relative contribution of I_h and I_M will depend on the exact value of V_{rest}. Thus, I_h is the main contributor to the mAHP at V_{rest} when it is negative to ∼−72 mV (Figs 11*C* and 12*C*). This U-shaped voltage-dependence is strongly reminiscent of the similarly shaped voltage-dependence of theta (θ) resonance in CA1 pyramidal cells (Hu *et al.* 2002*b*). Indeed, the underlying mechanisms are very similar. In both cases the amplitudes (of θ oscillations or mAHPs) are largest when either I_M (at depolarized V_m) or I_h (at hyperpolarized V_m) is strong, due to the *V* dependence of their activation and/or their driving forces, whereas the amplitude is minimal in the 'no man's land' in between, where neither I_M nor I_h is strongly activated and has a strong driving force. However, there is also an interesting difference: whereas the *V* dependence of channel activation is crucial for the U-shaped *V* dependence of the subthreshold resonance, the similarly shaped *V* dependence of the spike-evoked mAHP, is only partly due to the *V* dependence of *activation*. Since I_M mainly activates during the spike, and the spike amplitude is more than sufficient to traverse the full activation range of I_M, the *V* dependence of the M-mAHP is probably mainly due to the *V* dependence of I_M *driving force*, whereas the *V* dependence of the H-mAHP (which is little influenced by the spike) is mainly due to the *V* dependence of I_h *activation*.

These results are in good agreement with our recent data from genetic suppression of KCNQ/M-channels in mice (Hu *et al.* 2002*a*; Peters *et al.* 2005). In the mice, the mAHP at depolarized membrane potentials was largely eliminated by suppression of I_M, whereas the mAHP at hyperpolarized potentials was not affected.

In addition to the I_M and I_h underlying the mAHP, we have recently also found indications that the persistent Na^+ current, I_{NaP}, can further modulate the amplitude of the mAHP and other AHPs in CA1 pyramidal cells (Vervaeke *et al.* 2004). This effect will be described in detail in a separate article (manuscript submitted).

Functional importance of mAHP and its underlying currents

Although the main aim of this study was to determine the mechanisms underlying the mAHP, our results also have implications for possible functional roles of these mechanisms for the firing behaviour of CA1 pyramidal cells. In particular, they suggest that I_M and I_h will not only cause θ resonance in the subthreshold voltage range, as shown previously (Hu *et al.* 2002*b*), but will also favour AP firing in the θ frequency range. Thus, because the mAHP that follows each AP causes a period of relative refractoriness lasting about 150 ms, it should tend to promote discharge frequencies around 7 Hz (i.e. θ), e.g. in response to steady depolarization or asynchronous excitatory input of moderate intensity. This idea fits well with the observation that KCNQ2 subunits are localized to key sites for control of neuronal network oscillations and synchronization in the brain (Cooper *et al.* 2001). We are presently further exploring such 'suprathreshold θ resonance'.

Blockade of I_M and, hence, the mAHP by XE991, uncovered or enhanced the ADP (Fig. 6). Often, but not always, the enhanced ADPs triggered spike doublets or burst discharges (Fig. 6), indicating that I_M normally limits the occurrence of bursting (Yue & Yaari, 2004). As pointed out previously, the transition from single spikes to bursts dramatically boosts the impact of the cell on postsynaptic target neurones (Lisman, 1997). The XE991-induced bursts are reminiscent of complex spikes recorded from CA1 pyramidal cells rats during learning tasks, and bursting greatly enhances long-term synaptic potentiation (Ranck, 1973; Otto *et al.* 1991; Thomas *et al.* 1998; Pike *et al.* 1999; Yue & Yaari, 2004). As suggested (Yue & Yaari, 2004), the effects of Kv7/KCNQ/M-channel blockers on neuronal bursting may help to explain why these drugs are able to improve performance in memory tasks under certain conditions (Aiken *et al.* 1996).

Since both I_M and I_h are targets of modulation by multiple neurotransmitters and -modulators (Brown, 1988; Storm, 1990; Pape, 1996), both the mAHP amplitude and time course, as well as the relative contribution of the two currents at each membrane potential, and the occurrence of ADPs and bursting, are expected to undergo similar modulatory changes. Ascending monoaminergic pathways from the brainstem (locus coerulus, raphe nuclei, ventral tegmental area) and cholinergic input from the basal forebrain (medial septum/diagonal band) are known to mediate changes in the functional state of the forebrain, from sleep and drowsiness to arousal, wakefulness and attention (Steriade *et al.* 1993). Accordingly, monoamine transmitters such as noradrenaline, serotonin, histamine or dopamine, by shifting the activation curve of I_h to more a depolarized voltage range (Pedarzani & Storm, 1995; Pape, 1996), could cause this current to contribute

more to the generation of mAHPs at relatively depolarized potentials, together with I_M Cholinergic input could have a similar effect by shifting the voltage dependence of I_h (Luthi & McCormick, 1999), while having an opposite effect at depolarized potentials, suppressing the M-mAHP by blocking I_M (Halliwell & Adams, 1982). Thus, the dual mechanisms of the mAHP (Storm, 1989) imply multiple possibilities for tuning of the rhythmic network activity through neuromodulation.

Finally, the differential subcellular distribution of M- and h-channels, with high densities of h-channels in the distal dendrites (Magee, 1998; Lorincz *et al.* 2002), and possibly more M-channels in the axon, soma and proximal dendrites (Shah *et al.* 2002; Yus-Najera *et al.* 2003; Devaux *et al.* 2004), will have implications for the mAHP mechanisms and functions in different parts of the cell and under various physiological circumstances, such as during hippocampal θ oscillations. These functional consequences also need to be explored further.

References

Abel HJ, Lee JC, Callaway JC & Foehring RC (2004). Relationships between intracellular calcium and afterhyperpolarizations in neocortical pyramidal neurons. *J Neurophysiol* **91**, 324–335.

Aiken SP, Zaczek R & Brown BS (1996). Pharmacology of the neurotransmitter release enhancer linopirdine (DuP 996), and insights into its mechanism of action. *Adv Pharmacol* **35**, 349–384.

Biervert C, Schroeder BC, Kubisch C, Berkovic SF, Propping P, Jentsch TJ & Steinlein OK (1998). A potassium channel mutation in neonatal human epilepsy. *Science* **279**, 403–406.

Bond CT, Maylie J & Adelman JP (1999). Small-conductance calcium-activated potassium channels. *Ann N Y Acad Sci* **868**, 370–378.

Borgatti R, Zucca C, Cavallini A, Ferrario M, Panzeri C, Castaldo P, Soldovieri MV, Baschirotto C, Bresolin N, Dalla BB, Taglialatela M & Bassi MT (2004). A novel mutation in KCNQ2 associated with BFNC, drug resistant epilepsy, and mental retardation. *Neurology* **63**, 57–65.

Borg-Graham L (1999). Interpretations of data and mechanisms for hippocampal pyramidal cell models. In *Cerebral Cortex*, vol. 12, *Cortical Models*, ed. Jones EG, Ulinski PS & Peter A. Plenum Press, New York.

Brown DA (1988). M currents. *Ion Channels* **1**, 55–94.

Buzsaki G (2002). Theta oscillations in the hippocampus. *Neuron* **33**, 325–340.

Cai X, Liang CW, Muralidharan S, Kao JP, Tang CM & Thompson SM (2004). Unique roles of SK and Kv4.2 potassium channels in dendritic integration. *Neuron* **44**, 351–364.

Cingolani LA, Gymnopoulos M, Boccaccio A, Stocker M & Pedarzani P (2002). Developmental regulation of small-conductance Ca^{2+}-activated K^+ channel expression and function in rat Purkinje neurons. *J Neurosci* **22**, 4456–4467.

Cooper EC, Harrington E, Jan YN & Jan LY (2001). M channel KCNQ2 subunits are localized to key sites for control of neuronal network oscillations and synchronization in mouse brain. *J Neurosci* **21**, 9529–9540.

Devaux JJ, Kleopa KA, Cooper EC & Scherer SS (2004). KCNQ2 is a nodal K^+ channel. *J Neurosci* **24**, 1236–1244.

DiFrancesco D (1986). Characterization of single pacemaker channels in cardiac sino-atrial node cells. *Nature* **324**, 470–473.

DiFrancesco D (1995). Cardiac pacemaker: 15 years of 'new' interpretation. *Acta Cardiol* **50**, 413–427.

Dragoi G, Harris KD & Buzsaki G (2003). Place representation within hippocampal networks is modified by long-term potentiation. *Neuron* **39**, 843–853.

Faber ES & Sah P (2003). Calcium-activated potassium channels: multiple contributions to neuronal function. *Neuroscientist* **9**, 181–194.

Foehring RC, Schwindt PC & Crill WE (1989). Norepinephrine selectively reduces slow Ca^{2+}- and Na^+-mediated K^+ currents in cat neocortical neurons. *J Neurophysiol* **61**, 245–256.

Goh JW & Pennefather PS (1987). Pharmacological and physiological properties of the after-hyperpolarization current of bullfrog ganglion neurones. *J Physiol* **394**, 315–330.

Graham LJ (2004). The Surf-Hippo neuron simulation system, v3.5a, (www.neurophys.biomedicale.univ-paris5.fr/~graham/surf-hippo.html).

Gu N, Vervaeke K, Hu H & Storm JF (2003). M- and H-channels, but not SK channels, generate the medium afterhyperpolarization (mAHP) following spike bursts in hippocampal pyramidal cells. *Abstr Soc Neurosci* 53.1.

Gu N, Vervaeke K, Hu H & Storm JF (2004). M- and h-channels, but not SK channels, generate the medium afterhyperpolarization (mAHP) following single spikes and spike bursts in CA1 hippocampal pyramidal cells. *FENS Abstr* **2**, A082.6.

Halliwell JV & Adams PR (1982). Voltage-clamp analysis of muscarinic excitation in hippocampal neurons. *Brain Res* **250**, 71–92.

Hille B (2001). *Ion Channels of Excitable Membranes*, 3rd edn. Sinauer Associates, Sunderland, MA, USA.

Holscher C, Anwyl R & Rowan MJ (1997). Stimulation on the positive phase of hippocampal theta rhythm induces long-term potentiation that can be depotentiated by stimulation on the negative phase in area CA1 *in vivo*. *J Neurosci* **17**, 6470–6477.

Hu H, Gu N & Storm JF (2004). Differential contribution of apamin-sensitive SK potassium channels to afterhyperpolarizations (mAHP) in subicular and CA1 rat hippocampal pyramidal neurons. *FENS Abstr* **2,** A082.7.

Hu H, Peters HC, Dehnhardt M, Engler G, Engel AK, Pongs O, Isbrandt D & Storm JF (2002*a*). Suppression of M-current-mediating KCNQ channels in transgenic mice causing hyperexcitability and abnormal resonance behavior in hippocampus and neocortex. *Abstr Soc Neurosci* 438.9.

Hu H, Vervaeke K & Storm JF (2002*b*). Two forms of electrical resonance at theta frequencies, generated by M-current, h-current and persistent Na^+ current in rat hippocampal pyramidal cells. *J Physiol* **545**, 783–805.

Jensen MS, Azouz R & Yaari Y (1996). Spike after-depolarization and burst generation in adult rat hippocampal CA1 pyramidal cells. *J Physiol* **492**, 199–210.

Jensen O & Lisman JE (2000). Position reconstruction from an ensemble of hippocampal place cells: contribution of theta phase coding. *J Neurophysiol* **83**, 2602–2609.

Jentsch TJ (2000). Neuronal KCNQ potassium channels: physiology and role in disease. *Nat Rev Neurosci* **1**, 21–30.

Jentsch TJ, Schroeder BC, Kubisch C, Friedrich T & Stein V (2000). Pathophysiology of KCNQ channels: neonatal epilepsy and progressive deafness. *Epilepsia* **41**, 1068–1069.

Johnson SW & Seutin V (1997). Bicuculline methiodide potentiates NMDA-dependent burst firing in rat dopamine neurons by blocking apamin-sensitive Ca^{2+}-activated K^+ currents. *Neurosci Lett* **231**, 13–16.

Kandel ER & Spencer WA (1961). Electrophysiology of hippocampal neurons. II. After-potentials and repetitive firing. *J Neurophysiol* **24**, 243–259.

Kohler M, Hirschberg B, Bond CT, Kinzie JM, Marrion NV, Maylie J & Adelman JP (1996). Small-conductance, calcium-activated potassium channels from mammalian brain. *Science* **273**, 1709–1714.

Lancaster B & Nicoll RA (1987). Properties of two calcium-activated hyperpolarizations in rat hippocampal neurones. *J Physiol* **389**, 187–203.

Lancaster B & Pennefather P (1987). Potassium currents evoked by brief depolarizations in bull-frog sympathetic ganglion cells. *J Physiol* **387**, 519–548.

Lanthorn T, Storm J & Andersen P (1984). Current-to-frequency transduction in CA1 hippocampal pyramidal cells: slow prepotentials dominate the primary range firing. *Exp Brain Res* **53**, 431–443.

Lerche C, Scherer CR, Seebohm G, Derst C, Wei AD, Busch AE & Steinmeyer K (2000). Molecular cloning and functional expression of KCNQ5, a potassium channel subunit that may contribute to neuronal M-current diversity. *J Biol Chem* **275**, 22395–22400.

Lesage F, Guillemare E, Fink M, Duprat F, Heurteaux C, Fosset M, Romey G, Barhanin J & Lazdunski M (1995). Molecular properties of neuronal G-protein-activated inwardly rectifying K^+ channels. *J Biol Chem* **270**, 28660–28667.

Lisman JE (1997). Bursts as a unit of neural information: making unreliable synapses reliable. *Trends Neurosci* **20**, 38–43.

Lorincz A, Notomi T, Tamas G, Shigemoto R & Nusser Z (2002). Polarized and compartment-dependent distribution of HCN1 in pyramidal cell dendrites. *Nat Neurosci* **5**, 1185–1193.

Luthi A & McCormick DA (1999). Ca^{2+}-mediated up-regulation of I_h in the thalamus. How cell-intrinsic ionic currents may shape network activity. *Ann N Y Acad Sci* **868**, 765–769.

Maccaferri G, Mangoni M, Lazzari A & DiFrancesco D (1993). Properties of the hyperpolarization-activated current in rat hippocampal CA1 pyramidal cells. *J Neurophysiol* **69**, 2129–2136.

Madison DV, Lancaster B & Nicoll RA (1987). Voltage clamp analysis of cholinergic action in the hippocampus. *J Neurosci* **7**, 733–741.

Madison DV & Nicoll RA (1984). Control of the repetitive discharge of rat CA1 pyramidal neurons in vitro. *J Physiol* **354**, 319–331.

Madison DV & Nicoll RA (1986). Cyclic adenosine 3′,5′-monophosphate mediates beta-receptor actions of noradrenaline in rat hippocampal pyramidal cells. *J Physiol* **372**, 245–259.

Magee JC (1998). Dendritic hyperpolarization-activated currents modify the integrative properties of hippocampal CA1 pyramidal neurons. *J Neurosci* **18**, 7613–7624.

Main MJ, Cryan JE, Dupere JR, Cox B, Clare JJ & Burbidge SA (2000). Modulation of KCNQ2/3 potassium channels by the novel anticonvulsant retigabine. *Mol Pharmacol* **58**, 253–262.

Martire M, Castaldo P, D'Amico M, Preziosi P, Annunziato L & Taglialatela M (2004). M channels containing KCNQ2 subunits modulate norepinephrine, aspartate, and GABA release from hippocampal nerve terminals. *J Neurosci* **24**, 592–597.

McCormick DA & Huguenard JR (1992). A model of the electrophysiological properties of thalamocortical relay neurons. *J Neurophysiol* **68**, 1384–1400.

Melyan Z, Wheal HV & Lancaster B (2002). Metabotropic-mediated kainate receptor regulation of I_{sAHP} and excitability in pyramidal cells. *Neuron* **34**, 107–114.

Mermelstein PG, Song WJ, Tkatch T, Yan Z & Surmeier DJ (1998). Inwardly rectifying potassium (I_{RK}) currents are correlated with I_{RK} subunit expression in rat nucleus accumbens medium spiny neurons. *J Neurosci* **18**, 6650–6661.

Norris CM, Halpain S & Foster TC (1998). Reversal of age-related alterations in synaptic plasticity by blockade of L-type Ca^{2+} channels. *J Neurosci* **18**, 3171–3179.

O'Keefe J & Recce ML (1993). Phase relationship between hippocampal place units and the EEG theta rhythm. *Hippocampus* **3**, 317–330.

Otto T, Eichenbaum H, Wiener SI & Wible CG (1991). Learning-related patterns of CA1 spike trains parallel stimulation parameters optimal for inducing hippocampal long-term potentiation. *Hippocampus* **1**, 181–192.

Pape HC (1994). Specific bradycardic agents block the hyperpolarization-activated cation current in central neurons. *Neuroscience* **59**, 363–373.

Pape HC (1996). Queer current and pacemaker: the hyperpolarization-activated cation current in neurons. *Annu Rev Physiol* **58**, 299–327.

Pape HC & Driesang RB (1998). Ionic mechanisms of intrinsic oscillations in neurons of the basolateral amygdaloid complex. *J Neurophysiol* **79**, 217–226.

Pedarzani P, Krause M, Haug T, Storm JF & Stuhmer W (1998). Modulation of the Ca^{2+}-activated K^+ current sIAHP by a phosphatase-kinase balance under basal conditions in rat CA1 pyramidal neurons. *J Neurophysiol* **79**, 3252–3256.

Pedarzani P & Storm JF (1993). PKA mediates the effects of monoamine transmitters on the K^+ current underlying the slow spike frequency adaptation in hippocampal neurons. *Neuron* **11**, 1023–1035.

Pedarzani P & Storm JF (1995). Protein kinase A-independent modulation of ion channels in the brain by cyclic AMP. *Proc Natl Acad Sci U S A* **92**, 11716–11720.

Pennefather P, Lancaster B, Adams PR & Nicoll RA (1985). Two distinct CA-dependent K currents in bullfrog sympathetic ganglion cells. *Proc Natl Acad Sci U S A* **82**, 3040–3044.

Peters HC, Hu H, Pongs O, Storm JF & Isbrandt D (2005). Conditional transgenic suppression of M channels in mouse brain reveals functions in neuronal excitability, resonance and behavior. *Nat Neurosci* **8**, 51–60.

Pike FG, Meredith RM, Olding AW & Paulsen O (1999). Rapid report: postsynaptic bursting is essential for 'Hebbian' induction of associative long-term potentiation at excitatory synapses in rat hippocampus. *J Physiol* **518**, 571–576.

Pineda JC, Galarraga E, Bargas J, Cristancho M & Aceves J (1992). Charybdotoxin and apamin sensitivity of the calcium-dependent repolarization and the afterhyperpolarization in neostriatal neurons. *J Neurophysiol* **68**, 287–294.

Ranck JB Jr (1973). Studies on single neurons in dorsal hippocampal formation and septum in unrestrained rats. I. Behavioral correlates and firing repertoires. *Exp Neurol* **41**, 461–531.

Rundfeldt C & Netzer R (2000). Investigations into the mechanism of action of the new anticonvulsant retigabine. Interaction with GABAergic and glutamatergic neurotransmission and with voltage gated ion channels. *Arzneimittelforschung* **50**, 1063–1070.

Sah P (1996). Ca^{2+}-activated K^+ currents in neurones: types, physiological roles and modulation. *Trends Neurosci* **19**, 150–154.

Sah P & Faber ES (2002). Channels underlying neuronal calcium-activated potassium currents. *Prog Neurobiol* **66**, 345–353.

Sailer CA, Hu H, Kaufmann WA, Trieb M, Schwarzer C, Storm JF & Knaus HG (2002). Regional differences in distribution and functional expression of small-conductance Ca^{2+}-activated K^+ channels in rat brain. *J Neurosci* **22**, 9698–9707.

Schnee ME & Brown BS (1998). Selectivity of linopirdine (DuP 996), a neurotransmitter release enhancer, in blocking voltage-dependent and calcium-activated potassium currents in hippocampal neurons. *J Pharmacol Exp Ther* **286**, 709–717.

Schwindt PC, Spain WJ, Foehring RC, Stafstrom CE, Chubb MC & Crill WE (1988). Multiple potassium conductances and their functions in neurons from cat sensorimotor cortex in vitro. *J Neurophysiol* **59**, 424–449.

Selyanko AA, Hadley JK, Wood IC, Abogadie FC, Delmas P, Buckley NJ, London B & Brown DA (1999). Two types of K^+ channel subunit, Erg1 and KCNQ2/3, contribute to the M-like current in a mammalian neuronal cell. *J Neurosci* **19**, 7742–7756.

Shah MM, Mistry M, Marsh SJ, Brown DA & Delmas P (2002). Molecular correlates of the M-current in cultured rat hippocampal neurons. *J Physiol* **544**, 29–37.

Shao LR, Halvorsrud R, Borg-Graham L & Storm JF (1999). The role of BK-type Ca^{2+}-dependent K^+ channels in spike broadening during repetitive firing in rat hippocampal pyramidal cells. *J Physiol* **521**, 135–146.

Stackman RW, Hammond RS, Linardatos E, Gerlach A, Maylie J, Adelman JP & Tzounopoulos T (2002). Small conductance Ca^{2+}-activated K^+ channels modulate synaptic plasticity and memory encoding. *J Neurosci* **22**, 10163–10171.

Steriade M, McCormick DA & Sejnowski TJ (1993). Thalamocortical oscillations in the sleeping and aroused brain. *Science* **262**, 679–685.

Stocker M, Krause M & Pedarzani P (1999). An apamin-sensitive Ca^{2+}-activated K^+ current in hippocampal pyramidal neurons. *Proc Natl Acad Sci U S A* **96**, 4662–4667.

Storm JF (1987*a*). Action potential repolarization and a fast after-hyperpolarization in rat hippocampal pyramidal cells. *J Physiol* **385**, 733–759.

Storm JF (1987*b*). Potassium currents underlying afterhyperepolarizations (AHPs) and spike repolarization in rat hippocampal pyramidal cells (CA1). *Abstr Soc Neurosci* **13**, 176.

Storm JF (1988). Temporal integration by a slowly inactivating K^+ current in hippocampal neurons. *Nature* **336**, 379–381.

Storm JF (1989). An after-hyperpolarization of medium duration in rat hippocampal pyramidal cells. *J Physiol* **409**, 171–190.

Storm JF (1990). Potassium currents in hippocampal pyramidal cells. *Prog Brain Res* **83**, 161–187.

Takahashi T (1990). Membrane currents in visually identified motoneurones of neonatal rat spinal cord. *J Physiol* **423**, 27–46.

Tatulian L, Delmas P, Abogadie FC & Brown DA (2001). Activation of expressed KCNQ potassium currents and native neuronal M-type potassium currents by the anti-convulsant drug retigabine. *J Neurosci* **21**, 5535–5545.

Thomas MJ, Watabe AM, Moody TD, Makhinson M & O'Dell TJ (1998). Postsynaptic complex spike bursting enables the induction of LTP by theta frequency synaptic stimulation. *J Neurosci* **18**, 7118–7126.

Varnum MD, Busch AE, Bond CT, Maylie J & Adelman JP (1993). The min K channel underlies the cardiac potassium current IKs and mediates species-specific responses to protein kinase C. *Proc Natl Acad Sci U S A* **90**, 11528–11532.

Vervaeke K, Hu H & Storm JF (2004). An inhibitory action of subthreshold voltage dependent sodium channels: amplification of the medium and slow afterhyperpolarizations in CA1 pyramidal neurons. *FENS Abstr* A187.15.

Viana F, Bayliss DA & Berger AJ (1993). Multiple potassium conductances and their role in action potential repolarization and repetitive firing behavior of neonatal rat hypoglossal motoneurons. *J Neurophysiol* **69**, 2150–2163.

Villalobos C, Shakkottai VG, Chandy KG, Michelhaugh SK & Andrade R (2004). SKCa channels mediate the medium but not the slow calcium-activated afterhyperpolarization in cortical neurons. *J Neurosci* **24**, 3537–3542.

Wang Q, Curran ME, Splawski I, Burn TC, Millholland JM, VanRaay TJ, Shen J, Timothy KW, de Vincent GMJT, Schwartz PJ, Toubin JA, Moss AJ, Atkinson DL, Landes GM, Connors TD & Keating MT (1996). Positional cloning of a novel potassium channel gene: KVLQT1 mutations cause cardiac arrhythmias. *Nat Genet* **12**, 17–23.

Wang HS, Pan Z, Shi W, Brown BS, Wymore RS, Cohen IS, Dixon JE & McKinnon D (1998). KCNQ2 and KCNQ3 potassium channel subunits: molecular correlates of the M-channel. *Science* **282**, 1890–1893.

Williamson A & Alger BE (1990). Characterization of an early afterhyperpolarization after a brief train of action potentials in rat hippocampal neurons in vitro. *J Neurophysiol* **63**, 72–81.

Wittekindt OH, Visan V, Tomita H, Imtiaz F, Gargus JJ, Lehmann-Horn F, Grissmer S & Morris-Rosendahl DJ (2004). An apamin- and scyllatoxin-insensitive isoform of the human SK3 channel. *Mol Pharmacol* **65**, 788–801.

Yue C & Yaari Y (2004). KCNQ/M channels control spike afterdepolarization and burst generation in hippocampal neurons. *J Neurosci* **24**, 4614–4624.

Yus-Najera E, Munoz A, Salvador N, Jensen BS, Rasmussen HB, Defelipe J & Villarroel A (2003). Localization of KCNQ5 in the normal and epileptic human temporal neocortex and hippocampal formation. *Neuroscience* **120**, 353–364.

Acknowledgements

G.N. performed the sharp-electrode and whole-cell current-clamp experiments included in this study (including those presented in Figs 1–10, 13*C* and *D*, and S1); K.V. performed the computational modelling (illustrated in Figs 11 and 12, and 13*A* and *B*). H.H. performed the whole-cell voltage-clamp experiments (illustrated in Fig. 3*A* and *B*); J.F.S. performed pilot experiments (data not shown). We thank Lyle Graham, university Rene Descartes Paris, for the continuous development and support of the Surf-Hippo simulator, Paul Johannes Helm for help with our microscopes, and Cecilie Petterson Oksvold for expert technical assistance. This study was supported by the European Commission (Contract no. QLG3-1999-00827), and by the Norwegian Research Council (NFR) via the MH, FUGE, EMBIO and Norwegian Centre of Excellence programmes.

Supplemental material

The online version of this paper can be accessed at:
DOI: 10.1113/jphysiol.2005.086835
http://jp.physoc.org/cgi/content/full/jphysiol.2005.086835/DC1 and contains supplemental material consisting of a Computational Methods document and one supplementary figure.
This material can also be found as part of the full-text HTML version available from http://www.blackwell-synergy.com